Climate Dynamics
https://doi.org/10.1007/s00382-019-04959-y

Dynamical downscaling over the complex terrain of southwest South America: present climate conditions and added value analysis

Deniz Bozkurt[1] · Maisa Rojas[1,2] · Juan Pablo Boisier[1] · Roberto Rondanelli[1,2] · René Garreaud[1,2] · Laura Gallardo[1,2]

Received: 30 December 2018 / Accepted: 26 August 2019

Abstract
This study evaluates hindcast simulations performed with a regional climate model (RCM, RegCM4) driven by reanalysis data (ERA-Interim) over the Pacific coast and Andes Cordillera of extratropical South America. A nested domain configuration at 0.44° (~ 50 km) and 0.09° (~ 10 km) spatial resolutions is used for the simulations. RegCM4 is also driven by a global climate model (GCM, MPI-ESM-MR) on the same domain configuration to asses the added values for temperature and precipitation (historical simulations). Overall, both 10 km hindcast and historical simulation results are promising and exhibit a better representation of near-surface air temperature and precipitation variability compared to the 50 km simulations. High-resolution simulations suppress an overestimation of precipitation over the Andes Cordillera of northern Chile found with the 50 km simulations. The simulated daily temperature and precipitation extreme indices from 10 km hindcast simulation show a closer estimation of the observed fields. A persistent warm bias (~ +4 °C) over the Atacama Desert in 10 km hindcast simulation reveals the complexity in representing land surface and radiative processes over the desert. Difficulties in capturing the temperature trend in northern Chile are notable for both hindcast simulations. Both resolutions exhibit added values for temperature and precipitation over large parts of Chile, in particular, the 10 km resolves the coastal-valley Andes transitions over central Chile. Our results highlight that resolutions coarser than 50 km (e.g., GCMs and reanalysis) miss important climate gradients imposed by complex topography. Given that the highest spatial resolution of the current regional simulations over the South America is about 50 km, higher resolutions are important to improve our understanding of the dynamical processes that determine climate over complex terrain and extreme environments.

Keywords Model evaluation · Temporal-spatial scale analysis · Climate variability · Chile · Patagonia · Atacama Desert

1 Introduction

Regional-to-local scale climate information has become an issue of central importance, particularly to assess vulnerability to climate change and to integrate adaptation needs at regional and local levels. Given that global climate models (GCMs) generally fail to represent regional-scale features due to their coarse spatial resolutions (~ 100–200 km), a number of initiatives to coordinate regional climate model (RCM) simulations have arisen in recent years to provide regional-to-local scale climate change information. Within these initiatives, global multimodel programs such as the Coordinated Regional Downscaling Experiment (CORDEX) (Giorgi et al. 2009; Jones et al. 2011) are important to further improve the quality of the RCM results but also to explore the major shortcomings and strengths in the RCMs (Solman 2013).

Three important initiatives (CORDEX, CLARIS-LPB, CREMA) led to an important progress in RCM applications over the South America for RCM evaluation studies as well as for long-term climate variability with an emphasis on the Plata Basin, which is flat terrain at low altitude (Carril et al. 2012; Solman 2013; Solman et al. 2013; Coppola et al. 2014). In general, the finest spatial resolution used in these long-term RCM-based climate simulations is around 50 km.

Electronic supplementary material The online version of this article (https://doi.org/10.1007/s00382-019-04959-y) contains supplementary material, which is available to authorized users.

✉ Deniz Bozkurt
dbozkurt@dgf.uchile.cl

[1] Center for Climate and Resilience Research, University of Chile, Santiago, Chile

[2] Department of Geophysics, University of Chile, Santiago, Chile

Published online: 30 August 2019

In connection with this, some of the systematic biases such as precipitation overestimation over the mountain ranges were associated with the lack of resolving topographical forcing (Rojas 2006). Furthermore, using the CLARIS-LPB simulations, Solman (2013) emphasized that the horizontal resolution in the current climate simulations over South America is still too coarse to capture some regional features, and increased resolution may lead to better model performance, particularly over complex terrain. On the other hand, Rojas (2006) showed that higher resolution RCM simulations might still include precipitation overestimation over the southern Andes due to several factors such as biases in simulated water vapor content and topography, and physical configuration of the model.

Continental Chile, lying between the subtropical southeastern Pacific and the Andes Cordillera, extends from 18°S to 53°S and features an extremely complex terrain and diverse climate zones, which makes it difficult to resolve local-scale features in coarse- and medium-resolution climate model simulations. For instance, the Andes Cordillera, has a great influence on local-scale climate variability by acting as a climatic wall that disturbs airflow and moisture conditions on both sides of the barrier (Garreaud 2009). In an observational study, Viale and Garreaud (2015) showed that precipitation enhancement by orographic uplift on the windward side of the Andes produces large annual precipitation (> 2000 mm year^{-1}) in central-southern Chile. Further south in Chilean Patagonia ($\sim$ 40°S–55°S), the annual mean precipitation reaches 5000–10000 mm in the Patagonian Ice Fields due to the temperate, hyper-humid oceanic climate and orographic enhancement (Garreaud et al. 2013). On the other extreme of the country, northern Chile hosts the driest desert in the planet with a long-term mean annual precipitation typically below 5 mm in coastal areas (Middleton 2003; Garreaud et al. 2010). Rutllant et al. (2003) highlighted local-scale features such as the steep coastal topography, the adjacent cold ocean, and local circulations forced by the heating of the Andean slopes, as one of the main physical mechanisms that explain Atacama hyperaridity. In addition to local-scale features, large-scale circulation patterns such as El Niño-Southern Oscillation (ENSO) and Southern Annular Mode (SAM) play a key role on intraseasonal to interdecadal climate variability of Chile (e.g., Rutllant and Fuenzalida 1991; Silvestri and Vera 2009; Boisier et al. 2018).

To understand the interplay between the local- and large-scale climate in South America and Chile, a number of studies have been conducted on regional weather and climate model simulations. These studies mainly consist of dynamical downscaling of boundary conditions provided by reanalysis and cover a broad of spectrum of applications such as diagnostic studies (Viale et al. 2013; Garreaud et al. 2016), extreme hydrometeorological events (Bozkurt et al. 2016; Comin et al. 2018), and urbanization and air pollution aspects (Gallardo et al. 2002; Schmitz 2005; Saide et al. 2011; Mazzeo et al. 2018). Although numerical simulations in much of these studies were performed at high spatial resolution (a few km to 15 km) configurations, they cover a short period (e.g., days to months). In addition to these case studies, Lenaerts et al. (2014) used a high-resolution (5.5 km) RCM driven by reanalysis to describe the present-day (1979–2012) climate of Patagonia, and they showed that the RCM at 5.5 km is able to simulate the orographic uplift and precipitation generation, capturing the sharp climate gradients in the southern Andes. On the other hand, in addition to the high-resolution simulations driven by reanalysis, GCM-driven RCM simulations for the historical period should also be evaluated to fully assess the ability of RCMs, particularly to determine the degree of added value by means of resolving potential GCM errors through high-resolution topography and land-surface feedback. Only very recently, Falco et al. (2018) performed a comprehensive analysis of RCM evaluation together with the added value analysis at continental scale of South America based on the available CORDEX simulations at 50 km spatial resolution. In their added value analysis, Falco et al. (2018) concluded that results of the added value analysis of historical simulations with RCMs driven by CMIP5 models are inconclusive since added value is only found in certain regions and in limited simulations.

Given the general lack of RCM applications for model evaluation as well as added value analysis done with the GCM driven simulations, particularly at local scales, the first aim of this study is to evaluate high-resolution (10 km) hindcast simulations performed by an RCM (RegCM4) (Giorgi et al. 2012) forced by reanalysis for the period 1980–2015. The second aim of this paper is to determine the degree of added value by using historical GCM simulations (1975–2005) with the same RCM configuration used in the hindcast simulation. To our knowledge, this is the first time a comprehensive RCM evaluation effort is presented based on 10 km simulations focusing on the Pacific coast and the Andes Cordillera of extratropical South America. Furthermore, by taking the advantage of using nested domain technique with two different spatial resolutions of 0.44° ($\sim$ 50 km) and 0.09° ($\sim$ 10 km), we also analyze the impact of resolution on RCM performance in representing present climate conditions as well as on added value analysis. By doing this, we aim to establish confidence on the use of hindcast simulations and dynamically downscaled simulations using GCM projections.

In Sect. 2, we describe the experiment design, data and methodology. Section 3 presents the results of the model performance evaluation as well as the added value analysis through comparison of model simulations with the

observations. Section 4 summarizes the results and presents concluding remarks.

2 Model description, data and methodology

2.1 Model description and experiment design

In this study, we employed Regional Climate Model, version 4 (RegCM4), a three-dimensional, primitive equation, hydrostatic regional climate model developed by the International Centre for Theoretical Physics. RegCM4 was originally developed by Giorgi et al. (1993a, b) and its dynamical core is based on the hydrostatic version of the Penn State/NCAR mesoscale model MM5 (Grell et al. 1994). RegCM has been used in numerous regional climate model simulations, even over regions dominated by complex terrain features such as the Atacama Desert (Bozkurt et al. 2016), polar regions (Grassi et al. 2013; Bozkurt et al. 2018b), and European Alps (Giorgi et al. 2016). Multiple physical schemes are available in the model. In the present study RegCM4 runs are performed using (1) the land surface model Biosphere-Atmosphere Transfer Scheme (BATS) of Dickinson et al. (1993); (2) the planetary boundary layer of Holtslag et al. (1990); (3) the radiative scheme of the NCAR Community Climate System Model Version 3 (CCSM3) (Kiehl et al. 1996); (4) the ocean flux parameterization of Zeng et al. (1998); and the scheme of Pal et al. (2000) for representing resolvable precipitation. Based on a couple of test simulations done with different convective schemes (not shown), we employed the Grell scheme (Grell 1993) with a cumulus closure scheme of Fritsch and Chappell (Fritsch and Chappell 1980). More detailed description of the model and physical parameterizations can be found in Giorgi et al. (2012).

The modeling experiment consists of two nested domains at 0.44° (~ 50 km) and 0.09° (~ 10 km) spatial resolutions and 23 vertical levels with a one-way nesting approach (Fig. 1). The mother domain covers the whole South America continent and has 192 × 202 grid cells. The inner domain covers Chile, part of Argentina and the adjacent oceans, and has 320 × 520 grid cells based on a Rotated Mercator projection. For the hindcast simulations, initial and lateral boundary conditions for the mother domain were provided by the European Centre for Medium-Range Weather Forecasts (ECMWF) Reanalysis (ERA-Interim) dataset at 6-h intervals with a grid spacing of 0.75° × 0.75° (Dee et al. 2011). The nested domain simulation (hereafter RE10) was then forced by the 3D atmospheric outputs of the mother domain (hereafter RE50). Twelve grid points in each direction were allocated for each lateral buffer zone in which the models' prognostic variables were nudged to the boundary

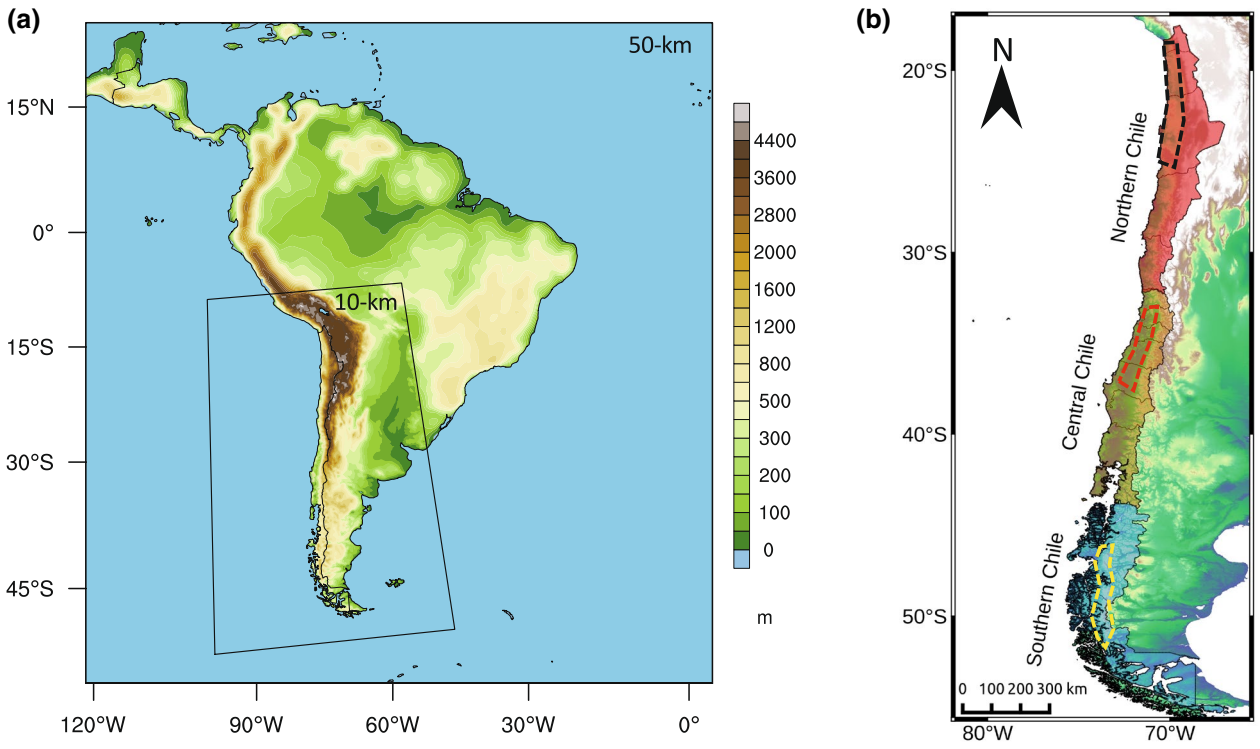

Fig. 1 **a** Mother and nested domain topography at 50 km and 10 km resolutions, respectively. **b** Three sub-regions used in this study. Dashed black, red and yellow borders identify the Atacama Desert, Central Valley and Patagonian Ice Fields, respectively

conditions with an exponential nudging coefficient proposed by Giorgi et al. (1993b). ERA-Interim sea surface temperature (SST) fields (6 hourly, 0.75° × 0.75°) were used as surface boundary conditions. The simulations were performed continuously from 1 January 1979 to 31 December 2015. First year of simulations (1979) was selected as spin-up period, and thus, not considered in the analysis.

In addition to the hindcast simulations, we performed historical simulations covering a period of 1976–2005 with lateral boundary conditions derived from MPI-ESM-MR, the Earth System Model of the Max Planck Institute for Meteorology at medium resolution. MPI-ESM-MR couples the atmosphere, ocean, sea-ice, and land and was used in a CMIP5-close configuration with spatial and vertical resolutions of T63 (~ 220 km) and L95, respectively (Giorgetta 2013). The same nested domain setup and physical configuration of the hindcast simulations were used in the historical simulations (hereafter RM50 for mother domain, RM10 for nested domain). RM50 and RM10 were then used to perform the added value analysis [see Sect. 2.3] for the period 1980–2005.

Summary of the simulations used in this study is given in Table 1. We mention that the selection criteria of the MPI-ESM-MR model within CMIP5 models is based on a comprehensive metric evaluation including large-scale circulation patterns, SST, ENSO and SAM variability in order to maximize correlations between these large-scale modes and the observed climate variability over Chile. Detailed information on selection criteria is given in supplementary material (Text S1, Fig. S1).

2.2 Data

Surface station data is provided by the Chilean National Weather Service (Dirección Meteorológica de Chile, DMC). A quality control and gap-filling procedures were applied to monthly station data [see Boisier et al. (2016)]. Due to the diverse climate features and high spatial climatic variability in Chile, the commonly used reference gridded products such as CRU are usually inadequate. For that reason, a high-resolution (CR2MET, 0.05° resolution) gridded meteorological dataset based on much denser station networks is used as the main reference dataset to evaluate RegCM4 performance and to perform added value analysis. CR2MET dataset contain gridded meteorological information of precipitation and temperature (mean, maximum and minimum) for the territory of continental Chile covering the period 1979–2016. In terms of precipitation, in addition to station data information, the CR2MET product is partly based on a statistical downscaling of ERA-Interim reanalysis. This approach, which is also based on station data information, includes multiple linear regression models to transfer precipitation, moisture fluxes and other variables from ERA-Interim onto 0.05° resolution precipitation estimates. The approach considers also local topography and is defined by a set of calibrated parameters with local rainfall observations. Regarding temperature, daily maximum and minimum temperatures were mapped onto the same grid resolution of 0.05° using land surface temperature (LST) estimates from MODIS satellite retrievals, in addition to near-surface temperature provided by ERA-Interim. Long-term maximum and minimum temperatures were used to adjust the ERA-Interim 3-hourly near-surface temperature so that the adjusted 3-hourly data were then used to derive the mean temperature. More detailed information about the CR2MET can be found in DGA (2017) and Alvarez-Garreton et al. (2018). The observed dataset used in this study is given in Table 1. In addition to the CR2MET, a catchment dataset of Chile (CAMELS-CL) (Alvarez-Garreton et al. 2018) is used to further assess the model evaluation by contrasting precipitation and runoff.

The simulation results were also compared with the driving fields from ERA-Interim. Evaporation product of GLEAM v3.2a (Martens et al. 2017) is used as a reference to evaluate the simulated evaporation over the northern Chile. Furthermore, energy balance components from CERES-EBAF-Surface v4 (Kato et al. 2013) are used as a reference dataset to further evaluate model performance over the Atacama Desert.

Table 1 List of the simulations and observed dataset used in this study

Name	Forcing	Period	Spatial resolution
Hindcast			
RE50	ERA-Interim Reanalysis	1979–2015	0.44 × 0.44° (~ 50 km)
RE10	RE50	1979–2015	0.09 × 0.09° (~ 10 km)
Historical			
RM50	MPI-ESM-MR	1975–2005	0.44 × 0.44° (~ 50 km)
RM10	RM50	1975–2005	0.09 × 0.09° (~ 10 km)
Observation and gridded products			
DMC-stations		1980–2015	
CR2MET		1980–2015	0.05 × 0.05° (~ 5 km)
ERA-Interim		1980–2015	0.75 × 0.75° (~ 80 km)

2.3 Methodology

Evaluation of RegCM4 model driven by ERA-Interim was firstly facilitated by using pressure level and surface variables. The simulation results were compared with driving fields from ERA-Interim to show the capability of the model to represent surface and pressure level characteristics in terms of mean sea level pressure (MSLP), 500 hPa geopotential height (z_{500}), 850 hPa wind vectors and specific humidity. Then, near-surface air temperature and precipitation fields were assessed using the available surface station data and gridded products. Mean biases, temporal correlation, and root mean square difference (RMSD) were used to evaluate the performance of RegCM4. Evaluation was also performed in terms of annual cycle and interannual variability of temperature and precipitation. Note that due to the diverse climate features, we used three subregions to look into the performance of the model: Northern Chile, Central Chile, and Southern Chile (see in Fig. 1b). Shapefiles of each region were used for masking, and only grids over the land areas were used for spatial-average comparisons. CR2MET was used as the reference observed dataset in these comparisons.

Model evaluation was also performed using the daily temperature and precipitation extreme indices following the definition of the expert team on climate change detection and indices (ETCCDI, Karl et al. 1999; Peterson et al. 2001). These include 90th percentile of daily maximum temperature (TX90), frost days (FD), 95th percentile of daily precipitation at wet days (R95), and consecutive dry days (CDD). All indices were calculated using the data for the entire year. Simulated temperature and precipitation indices of RE50 and RE10 were assessed against the CR2MET dataset. Detailed definitions of the indices used in this study are listed in Table 2. A full descriptive list of the indices can be found on the ETCCDI website http://etccdi.pacificclimate.org/list_27_indices.shtml.

To ease comparison between model simulations and observations, we used 0.44° resolution as a common grid, therefore, high resolution dataset of CR2MET and RE10 were upscaled to the 0.44° resolution. In order to have the exact grid numbers, temperature fields from each dataset including RE50 and ERA-Interim too, were interpolated onto the 0.44° resolution using bilinear interpolation. Additionally, an elevation correction was carried out for temperature assuming a uniform temperature lapse of 0.65 °C/100 m, using the CR2MET topography as reference, after regridding onto the common grid. In terms of precipitation, we used first order conservative remapping method that conserves the total area integral of the precipitation (Jones 1999). This technique is assumed to be appropriate for analysis of precipitation fluxes at different resolution grids (e.g., Di Luca et al. 2013; Guttler et al. 2015). No attempt was made to correct the precipitation based on the elevation differences.

A further analysis of the simulations was performed using the added value metric, which shows the squared error differences between the lateral boundary conditions provided by MPI-ESM-MR and the downscaled RegCM4 output. It is calculated as follows (adopting from Di Luca et al. (2016)):

$$AV = \frac{(X_{GCM} - X_{OBS})^2 - (X_{RCM} - X_{OBS})^2}{Max\left((X_{GCM} - X_{OBS})^2, (X_{RCM} - X_{OBS})^2\right)} \quad (1)$$

where X_{GCM} is the boundary conditions from MPI-ESM-MR, X_{OBS} is the observed reference dataset (CR2MET), and X_{RCM} is the downscaled RegCM4 output driven by MPI-ESM-MR. X in this study corresponds to the temporal mean (1980–2005) of temperature and precipitation on an annual basis. Positive values (AV > 0) indicate the grids that show added value provided by dynamical downscaling with RegCM4.

As all variables must be on the same grid for added value, we used three representative grid resolutions of 0.44°, 1° and 1.5° resolutions. In order to minimize uncertainties and possible errors arising from regridding, particularly when upscaling from high resolution dataset of CR2MET and RM10, we gradually regridded each dataset following the same methodology performed by Torma et al. (2015). In other words, three common grids are used as intermediate resolutions, and for instance, CR2MET and RM10 were upscaled to the multiple low resolutions (0.44°, 1°, and 1.5° resolutions) step by step. We used bilinear and first order conservative remapping for temperature and precipitation, respectively. We applied the same approach of elevation correction for temperature fields of RM10, RM50 and MPI-ESM-MR fields after regridding. Given that we are using three different sub-regions of Chile in a narrow area characterized by complex terrain, 1.5° grid resolution does not have enough number of grids in the sub-regions to assess and quantify the simulation results. Therefore, we only provide results from 0.44° and 1° grid resolutions.

Table 2 Definitions of extreme temperature and precipitation indices used in this study

Indice label	Indice name	Indice definition	Units
TX90	Extreme temperature	90th percentile of daily maximum temperature	°C
FD	Frost days	Number of days where daily minimum temperature < 0 °C	days
R95	Extreme precipitation	95th percentile of daily precipitation on wet days (R ≥ 1 mm)	mm
CDD	Consecutive dry days	Maximum number of consecutive dry days where R < 1 mm	days

3 Results

In this section, we first present the performance evaluation of RegCM4 model driven by ERA-Interim in terms of surface variables of temperature and precipitation (Sect. 3.1). We then present the added value analysis using the MPI-ESM-MR, RM10 and RM50 results (Sect. 3.2).

3.1 Performance of RegCM4

An evaluation of the large-scale circulation based on synoptic fields is provided in full detail in the supplementary material (Text S2, Figs. S2, S3). Overall, RegCM4 is capable of reproducing mean spatial fields of important large-scale features such as the Southeast Pacific Subtropical Anticyclone (SPSA), the mid-latitude westerly winds over the Patagonia and low-level moisture distribution along both sides of the Andes barrier. The higher resolution simulation (RE10) generally gives a better performance in terms of representing magnitude of these fields compared to those in RE50 at annual and summer time scales. Both simulations tend to have stronger westerlies compared to the ERA-Interim over the Patagonia.

3.1.1 Temperature regimes

Figure 2 shows the mean observed, ERA-Interim and simulated annual temperature distribution over the region for the period of 1980–2015. Surface station data indicate a distinct latitudinal distribution of the temperature with values lower than 10 °C in the southern Chile (42 °S and 55 °S) and 16 °C to 22 °C in central and northern Chile (Fig. 2a). Zonal temperature contrast also exists, particularly over the Altiplano sector in northern Chile with a temperature difference around 10 °C between the coastal areas and higher elevations. These spatial features are represented reasonably well in the gridded product of the CR2MET with finer local details of temperature such as Patagonian Ice Fields in the south and Salar de Atacama in the north (Fig. 2b). ERA-Interim yields a consistent temperature pattern with the CR2MET over Chile, yet it exhibit higher (+ 1 to + 5 °C) and lower (− 1 to − 5 °C) temperature ranges along the northern Chile coasts and over the Cordillera of central-northern Chile, respectively (Fig. 2c, also see in Fig. S4).

Overall, the downscaled simulations of ERA-Interim at two different spatial resolutions capture well the spatial pattern of mean annual temperature. Nonetheless, there are noticeable differences between the simulated and observed temperatures. Temperature distribution in RE50 illustrates a similar pattern to that in ERA-Interim, however, RE50 underestimates temperature over the central-southern Chile, particularly over the Cordillera of central-northern Chile (− 2 to − 5 °C) (Figs. 2d, S4). Compared to the RE50, RE10 generally reduces the cold bias over the Central Valley and Cordillera due to the finer topography. On the other hand, RE10 overestimates temperature in northern Chile, particularly in Atacama Desert (∼ 4 °C) (Fig. 2e, S4), while it tends to simulate colder temperatures over the southern Chile. RE50 represents a closer estimation of observed temperature over the Atacama Desert. However, this does not imply that RE50 has a better representation of the surface fluxes but rather it may include more systematic errors leading to wrong characterization of the temperature pattern over the desert. Indeed, RE10 gives a closer estimation and variability of evaporation to that in the reference dataset of GLEAMv3.2a over the Atacama Desert (Fig. S5a).

The Atacama warm bias in RE10 is further investigated using surface energy balance components. Figure 3 shows mean annual averaged of surface energy balance components (W $m2^{-1}$) over the Atacama Desert (see Fig. 1b) from CERES-EBAF-v4, RE50 and RE10. Both simulations have almost the same amount of net absorbed solar radiation at the surface with an underestimation compared to the estimated values of CERES-EBAF-v4 over the Atacama Desert. The warm surface temperature bias of RE10 is expected to lead to an overestimation of upwelling longwave radiation, however, it is underestimated compared to CERES-EBAF-v4 dataset. An overestimation exists in the simulated downwelling longwave radiation for RE10. Although this can be a consequence of the warm surface temperature bias, it could be argued that the overestimation of downwelling longwave radiation and associated underestimation of net radiative cooling in RE10 compared to the CERES-EBAF-v4 and RE50, can partially control the warm surface temperature bias. Furthermore, RE10 tends to have larger surface specific humidity values compared to those in the RE50 indicating a larger greenhouse effect locally (Fig. S5b). These discrepancies might be associated with lack of dust module and accurate land surface processes such as surface emissivity and albedo in the model configuration used in this study. Indeed, for instance, Marcella and Eltahir (2012) corrected a warm bias in RegCM3 simulations over semi-arid southwest Asia by modifying model's surface albedo values and incorporating RegCM3's dust module.

Figure 4 presents the mean annual cycle and interannual variability of temperature (1980–2015 period) from CR2MET, ERA-Interim and simulations for three subregions. Overall, both simulations at different resolutions illustrate a very close spatial-mean temperature climatology and variability in each subregion. However, some regional differences exist among the simulations. For instance, in northern Chile, RE50 shows an underestimation of temperature, while RE10 is characterized by a warm bias (close to + 1 °C) from January to March (Fig. 4a). Regarding the interannual variability of temperature, both simulations show a moderate

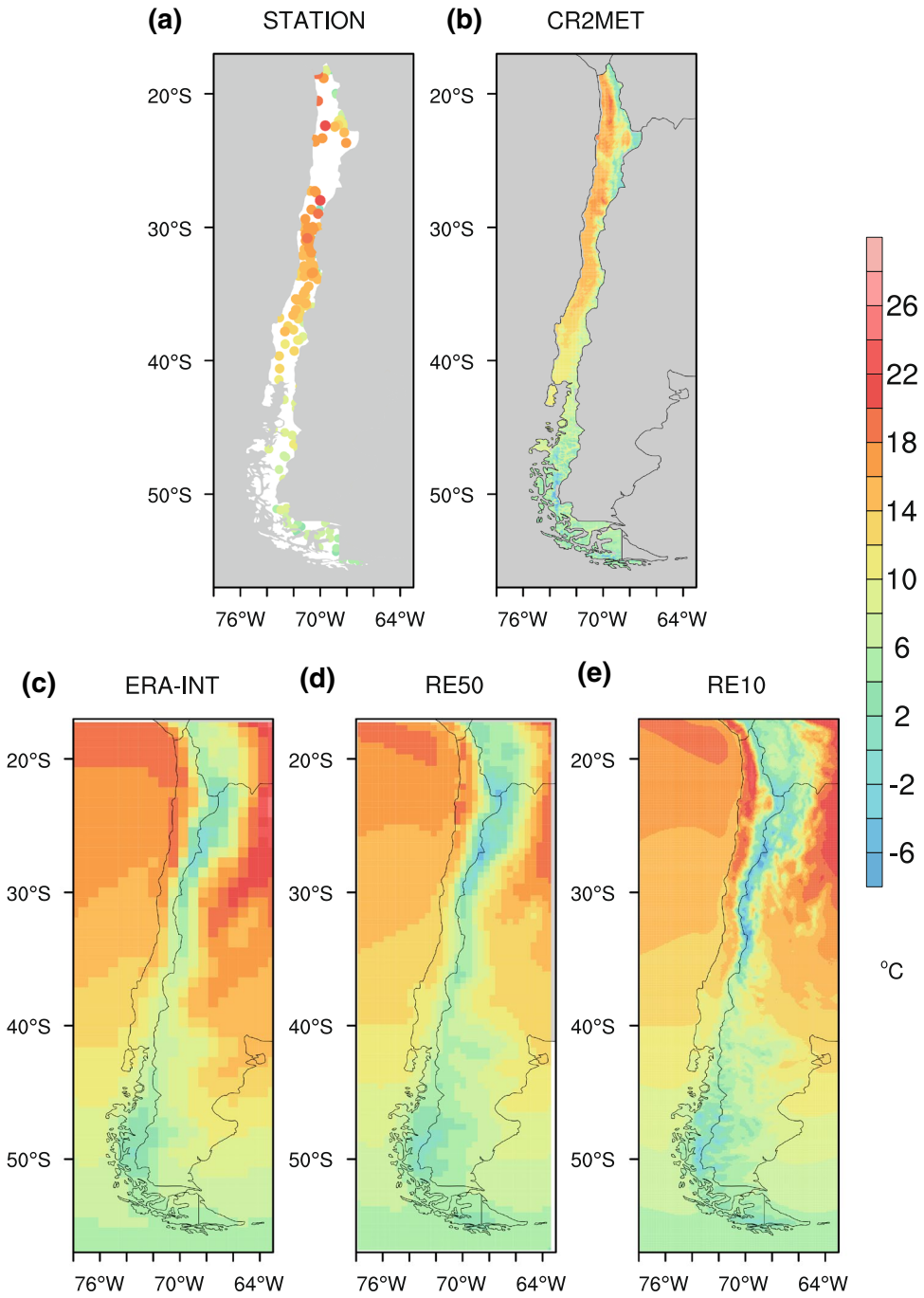

Fig. 2 **a** Spatial distribution of 36-year (1980–2015) mean annual average temperature (°C) from surface observations, **b** gridded observation (CR2MET), **c** ERA-Interim, **d** dynamically downscaled simulations of ERA-Interim at 50-km (RE50) and **e** 10-km (RE10) resolutions

temporal correlation with CR2MET (0.42 for RE50 and 0.45 for RE10) in northern Chile. RE10 has a better representation of temperature variability with lower bias and RMSD in central Chile. In southern Chile, both simulations have the highest temporal correlation among the three sub-regions (0.82 for RE50 and 0.83 for RE10), yet a systematic cold bias exist in both simulations with larger RMSD values in RE10

Large discrepancies between the observed and simulated temperature variability in northern Chile could be related to the recent cooling trend in coastal SST (Falvey and Garreaud 2009). Falvey and Garreaud (2009) showed a recent cooling trend ($-0.2\,^{\circ}\mathrm{C\ decade^{-1}}$) off the coast of northern and central Chile for the period 1979–2006. They also highlighted a strong contrast between surface cooling at coastal stations and warming in the Andes ($+0.25\,^{\circ}\mathrm{C\ decade^{-1}}$). Vuille et al. (2015) also illustrated the cooling along the coastal zone and warming in the Andes using station data. A trend map of observed and simulated temperature for the period 1980–2015 shows

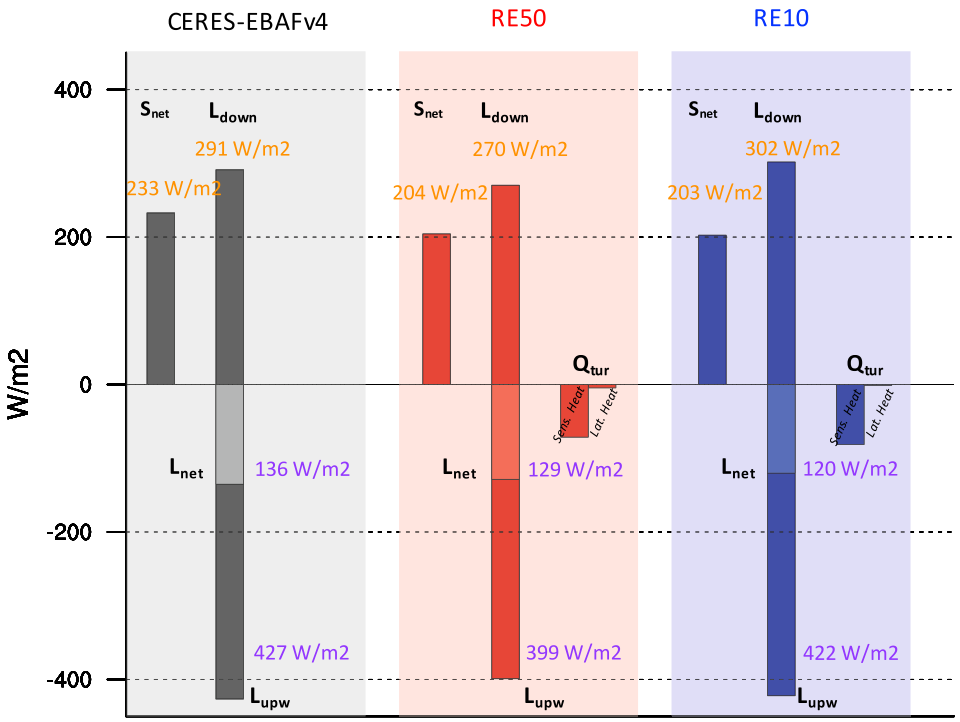

Fig. 3 Surface energy balance components (W $m2^{-1}$) over the Atacama Desert (see Fig. 1b) from CERES-EBAF-v4 (gray), dynamically downscaled simulations of ERA-Interim at 50-km (RE50, red) and 10-km (RE10, blue) resolutions. Values correspond to mean annual average for the period 2001-2015 for CERES-EBAF-v4, 1980-2015 for RE50 and RE10. S_{net}: Net shortwave radiation, L_{down}: Downward longwave radiation, L_{upw}: Upward longwave radiation, L_{net}: Net longwave radiation, Q_{tur}: Turbulent heat fluxes (i.e., sensible and latent heat fluxes)

that both RCM simulations capture the cooling trend (~ -0.1 to $-0.3\,^{\circ}$C decade^{-1}) in the coastal area, however, RE50 fails to capture the warming trend over most parts of the Andes while RE10 captures some observed warming trend over the central Andes ($\sim$ 28°S to $\sim$ 35°S) (Fig. 5c, d).

Difficulties in capturing the temperature variability in northern Chile result in poor performance of representing TX90 variability (e.g., very low correlations) for both simulations over this region (Fig. 6). Particularly, a systematic warm bias is clear in RE10. In central Chile, both simulations largely capture the interannual variability of TX90, however, RE50 exhibits a systematic underestimation ($\sim$ 2 °C). RE10 tends to have larger than observed TX90 on the broad areas of central Chile and Central Valley, and lower than observed TX90 over the Andes ranges as well as the Patagonian Ice Fields. A similar comparison of temperature extremes shows that both simulations capture well the FD variability, yet RE10 exhibits a better spatial and temporal variability of the FD over the southern Chile where the Patagonian Ice Fields are located (Fig. S6).

3.1.2 Precipitation regimes

Long-term mean (1980–2015) annual accumulated precipitation from the observed station data and gridded products as well as dynamically downscaled simulations are given in Fig. 7. Rain-gauge data shows the striking precipitation gradient increasing from north (< 100 mm) to south (> 600 mm) as well as from coastal areas ($\sim$ 1000 mm) to the Andes ($\sim$ 4000 mm) in central-southern Chile (Fig. 7a). CR2MET represents well the station-based spatial pattern of precipitation including north to south precipitation increase and orographic modification of the Andes in central-southern Chile (Fig. 7b).

ERA-Interim is characterized by the same north to south precipitation gradient with a slightly different magnitudes such as more precipitation in Patagonia and northern Chile (Fig. 7c). RE50 does not capture well the orographic enhancement of precipitation and shows a dry bias over the mountains areas of central-southern Chile (Figs. 7d, S7). Wetter conditions in the Central Valley zone and Andes ranges of northern Chile are also notable in RE50. On the other hand, RE10 captures the main features of the climatological pattern of precipitation such as latitudinal variation and orographic forcing. Particularly, RE10 enhances orographic forcing and reproduces precipitation increase reasonably well in western slope of the Andes in central-southern Chile (Fig. 7e). Compared to its forcing field of ERA-Interim, improvement of orographic precipitation in RE10 can also be seen in the bias map with respect to CR2MET (Fig. S7). On the other hand, RE10 tends to have a large standard deviation of annual accumulated precipitation

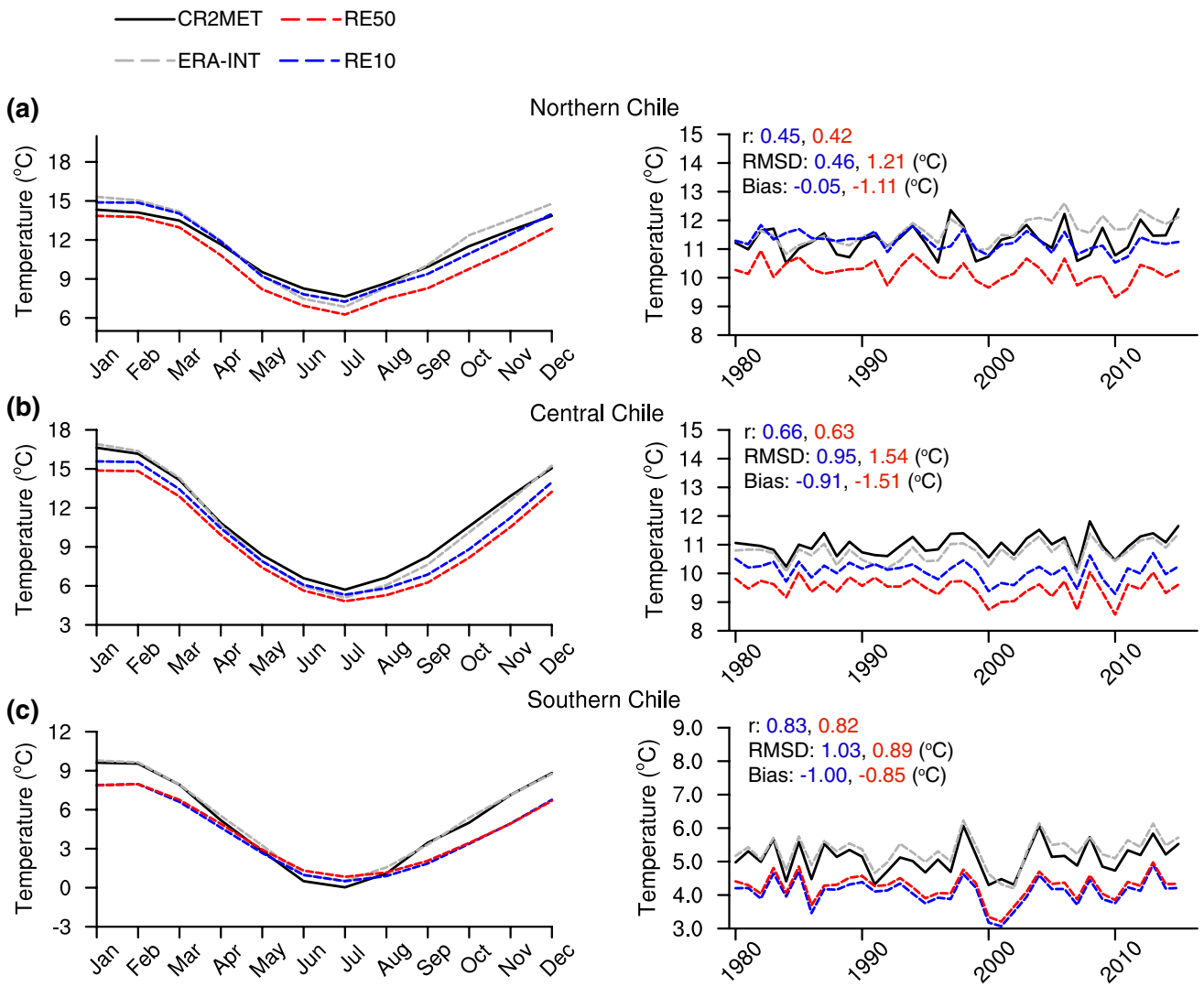

Fig. 4 **a** 36-year (1980–2015) mean annual cycle and inter-annual variability of temperature (°C) for Northern Chile, **b** Central Chile, **c** Southern Chile. The solid line corresponds to CR2MET (black), and the dashed lines correspond to ERA-Interim (gray), dynamically downscaled simulations of ERA-Interim at 50-km (RE50, red) and 10-km (RE10, blue) resolutions

(~ 1000 mm) on some grids within the Andes ranges of central Chile and Patagonian Ice Fields (Fig. S8a). Both simulations, however, capture well the spatial pattern of coefficient of variation with the largest values (0.6–0.9) in northern Chile (Fig. S8b).

The mean annual cycle and interannual variability of precipitation (1980–2015 period) for three sub-regions are given in Fig. 8. In northern Chile, overall, both simulations capture the observed annual cycle shape and interannual variability with a systematic overestimation. RE50 substantially overestimates the precipitation, on the other hand, RE10 closely agrees with the observed values and ERA-Interim, indicating the improvement of the model performance at finer resolution. In central Chile, spatial-mean precipitation climatology and interannual variability (e.g., El Niño and La Niño years) are well reproduced by both simulations indicating no significant performance improvement with higher resolution.

In recent years, central Chile has been experiencing a persistent deficit of precipitation (~ 30%) (Boisier et al. 2016), which is expected to continue in the future based on the climate projections (Demaria et al. 2013; Bozkurt et al. 2018a). This so-called mega-drought has caused significant impacts in surface hydrology and vegetation productivity in central Chile (Garreaud et al. 2017). A further comparison of the precipitation anomaly during the 2010–2015 period with respect to long-term mean shows that both simulations reasonably produce the spatial extent of the recent drying period (~ 30°S to ~ 40°S) (Fig. S9). Long-term (1980–2015) trend map of precipitation exhibits that the

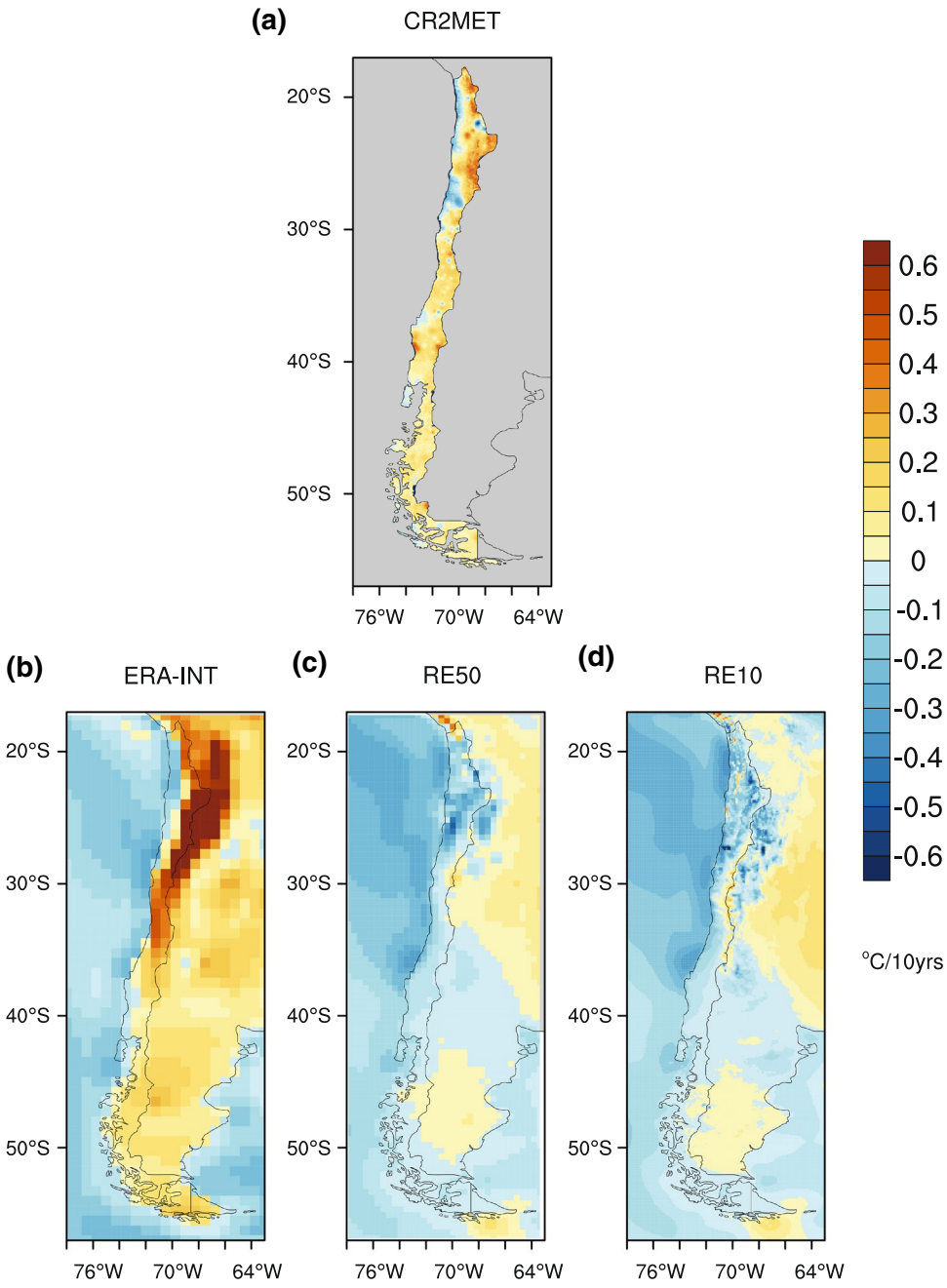

Fig. 5 (**a**) Trends in annual temperature (°C 10 yrs^{-1}) for the period 1980–2015 for CR2MET, (**b**) ERA-Interim, (**c**) dynamically downscaled simulations of ERA-Interim at 50-km (RE50) and (**d**) 10-km (RE10) resolutions

simulations, especially RE10, also capture the long-standing drying trend in central-southern Chile showed by Boisier et al. (2018) (Fig. S10).

A well-distributed pattern of precipitation along the year is captured by both simulations in southern Chile with a slight systematic underestimation. Both simulations successfully reproduce most of the interannual variability of precipitation in southern Chile, with a slightly better temporal correlation in RE10 (0.76) than that in RE50 (0.72).

To take a closer look at the simulated precipitation comparison, zonal variation of mean annual accumulated precipitation along four different latitudes (30°S, 35°S, 40°S and 45°S) is presented in Fig. 9. Overall, 10 km simulation results exhibit a better representation of precipitation variability and suppress an overestimation of precipitation over the Andes Cordillera of northern Chile found in the 50 km simulation. Furthermore, high-resolution simulations capture well the zonal precipitation variability over the coastal range and the upstream of the Andes range in central-southern Chile.

A further comparison was performed by means of runoff-precipitation covariability. Figure 10a presents the scatter diagram of long-term mean (1980–2015) precipitation from CR2MET versus observed runoff from CAMELS-CL

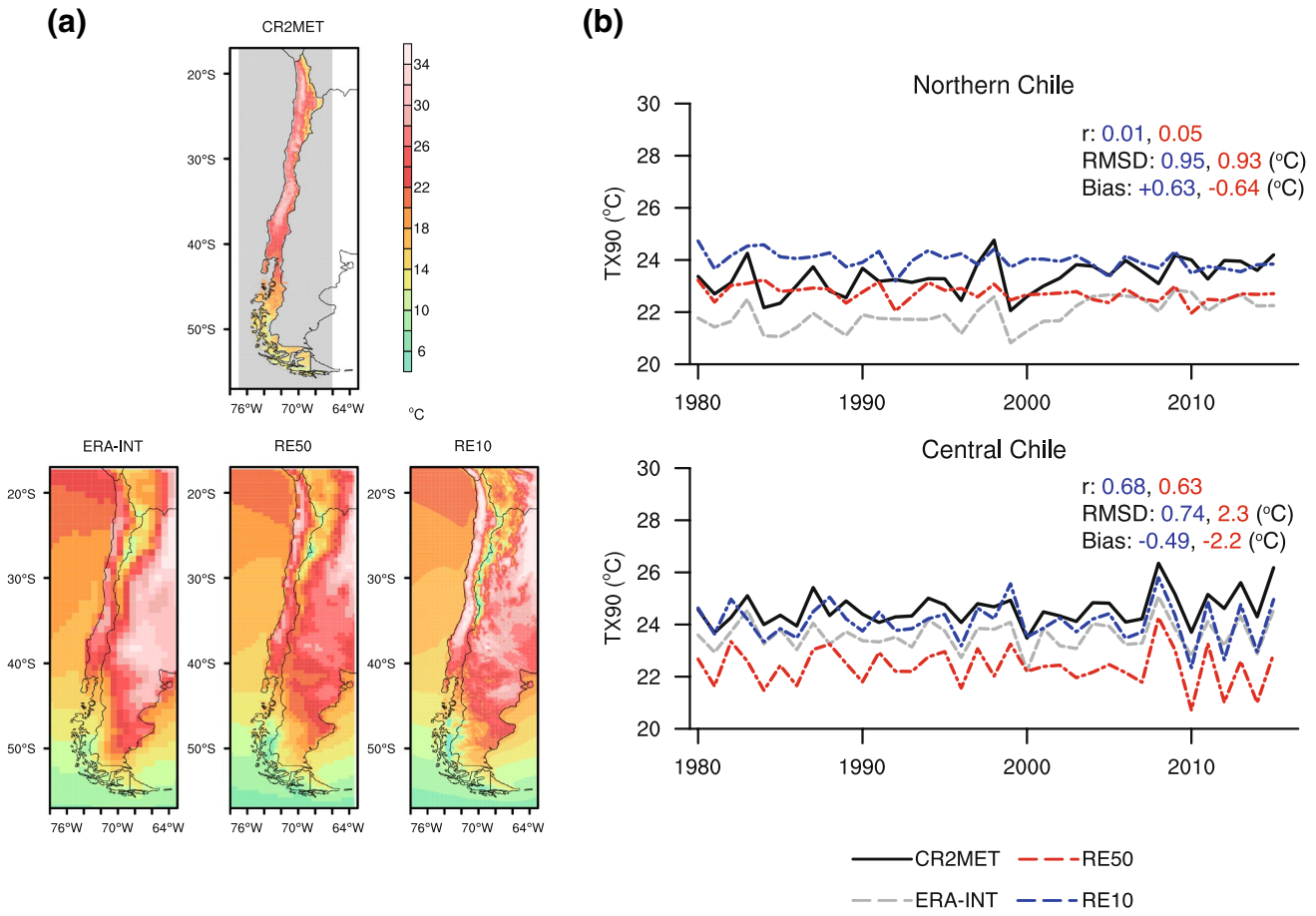

Fig. 6 (**a**) Spatial distribution of 36-year (1980–2015) mean annual TX90 (90th percentile of the daily maximum temperature, °C) from CR2MET, ERA-Interim, dynamically downscaled simulations of ERA-Interim at 50-km (RE50) and 10-km (RE10) resolutions. (**b**) Inter-annual variability of TX90 for Northern Chile and Central Chile. The solid line corresponds to CR2MET (black), and the dashed lines correspond to ERA-Interim (gray), RE50 (red) and RE10 (blue)

in central Chile. Overall, CR2MET reveals a close fit to the 1:1 line in central Chile ($R^2 = 0.87$) with runoff ratios (Runoff/Precipitation) ranging between expected values (0.5 and 0.8) (Alvarez-Garreton et al. 2018). However, there are some values with runoff ratios greater than 1 that indicate a precipitation underestimation assuming that streamflow data and catchment area are reliable (Alvarez-Garreton et al. 2018). RE50 gives relatively low runoff ratios (i.e., precipitation overestimation, see also Fig. S7) with a lower coefficient of determination (0.66) (Fig. 10b). RE10 exhibit a very similar scatter with CR2MET in which a close fit to the 1:1 line is kept (Fig. 10b). Compared to the RE50, RE10 gives a better representation of precipitation-runoff covariability with a larger R^2 value (0.83) indicating an improvement of the simulations with the use of higher spatial resolution. Similar to CR2MET, runoff ratios larger than 1 also exist in both simulations indicating the precipitation underestimation, which was also observed in different precipitation products (Alvarez-Garreton et al. 2018). Regarding the runoff-precipitation interannual covariability, CR2MET exhibits R^2 values larger than 0.6 in central Chile. RE50 shows a poorer performance with low R^2 values (< 0.5) while RE10 has a slightly better performance in representing the runoff-precipitation interannual covariability.

Finally we close this subsection with precipitation extremes. Long-term mean (1980–2015) R95 values from the observation, ERA-Interim and simulations are given in Fig. 11a. Observed R95 values of daily precipitation indicate that most parts of the Andes along with small spots in the Central Valley and Patagonian Ice Fields feature high daily precipitation values (> 60 mm), and largest values are concentrated around 35°S (~ 80 mm) over the Cordillera in central Chile. RE50 shows high R95 values (50–70 mm) mostly concentrated along the Central Valley zone and it does not represent the observed maximum of R95 over the central Andes ranges. On the other hand, RE10 captures well the spatial distribution of R95 maxima over the Andes ranges in

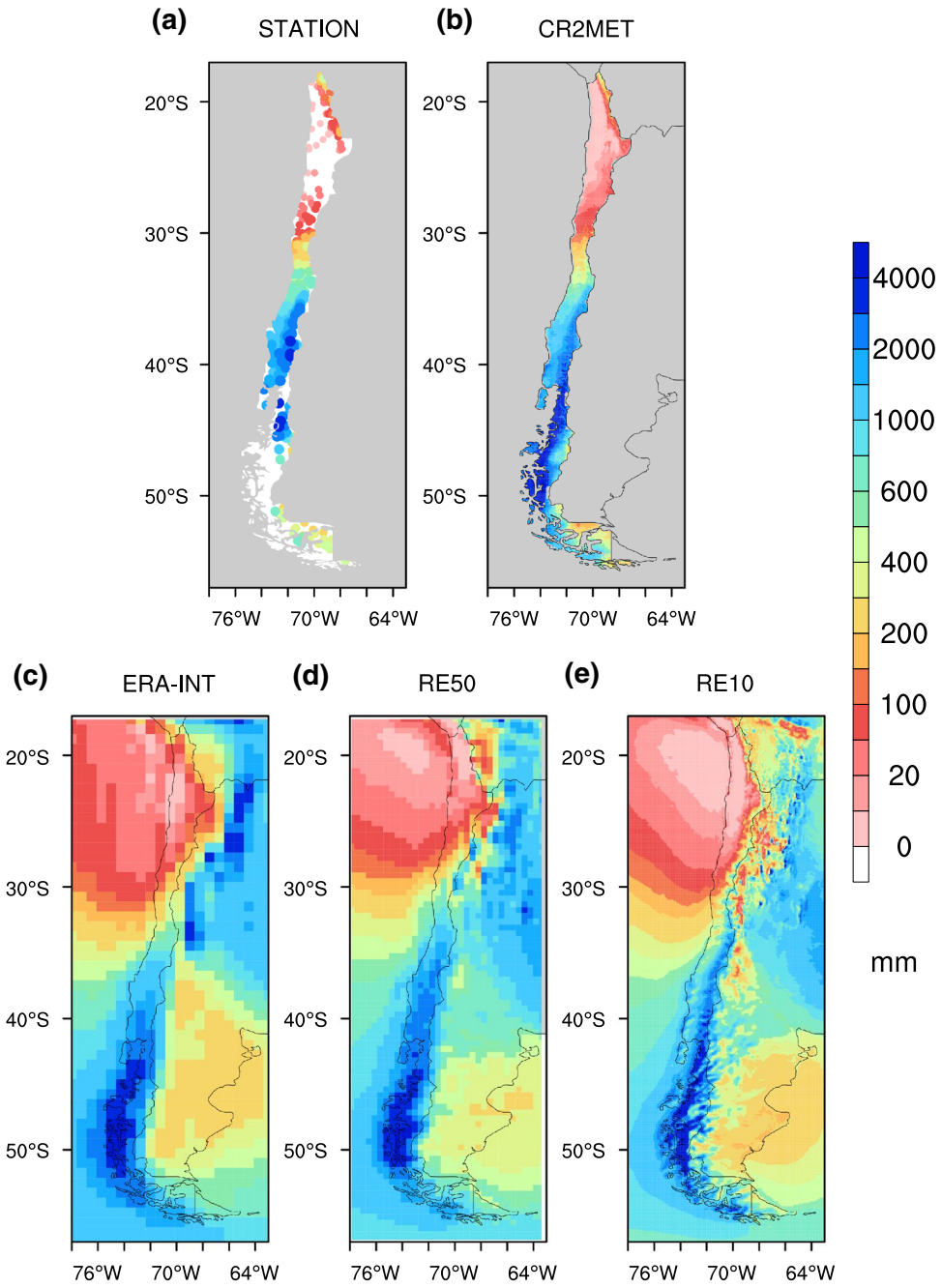

Fig. 7 **a** Spatial distribution of 36-year (1980–2015) mean annual total precipitation (mm) from surface observations, **b** gridded observation (CR2MET), **c** ERA-Interim, **d** dynamically downscaled simulations of ERA-Interim at 50-km (RE50) and **e** 10-km (RE10) resolutions

central Chile albeit notably larger than the observed values (> 90 mm). Both simulations show high skill in simulating interannual variability of R95 over central Chile representing the observed increasing and decreasing tendency of R95 during El Niño and La Niña years, respectively (e.g., 1997 and 1998) (Fig. 11b). However, a systematic overestimation of R95 exists in RE10 mainly due to the larger R95 over the Andes ranges in central Chile. In terms of CDD, both simulation follow closely forcing field of ERA-Interim and, overall there is a good consistency between the observed and simulated CDD patterns. However, the magnitude of CDD is underestimated (wetter conditions) over the Andes range of central and northern Chile (Fig. S11).

Overall, so far, long-term climatological analysis at daily, monthly, annual and seasonal scales show that RE10 has a better performance than RE50 in preserving the observed spatial and temporal variabilities, particularly for precipitation, despite some discrepancies in temperature variability over the northern Chile.

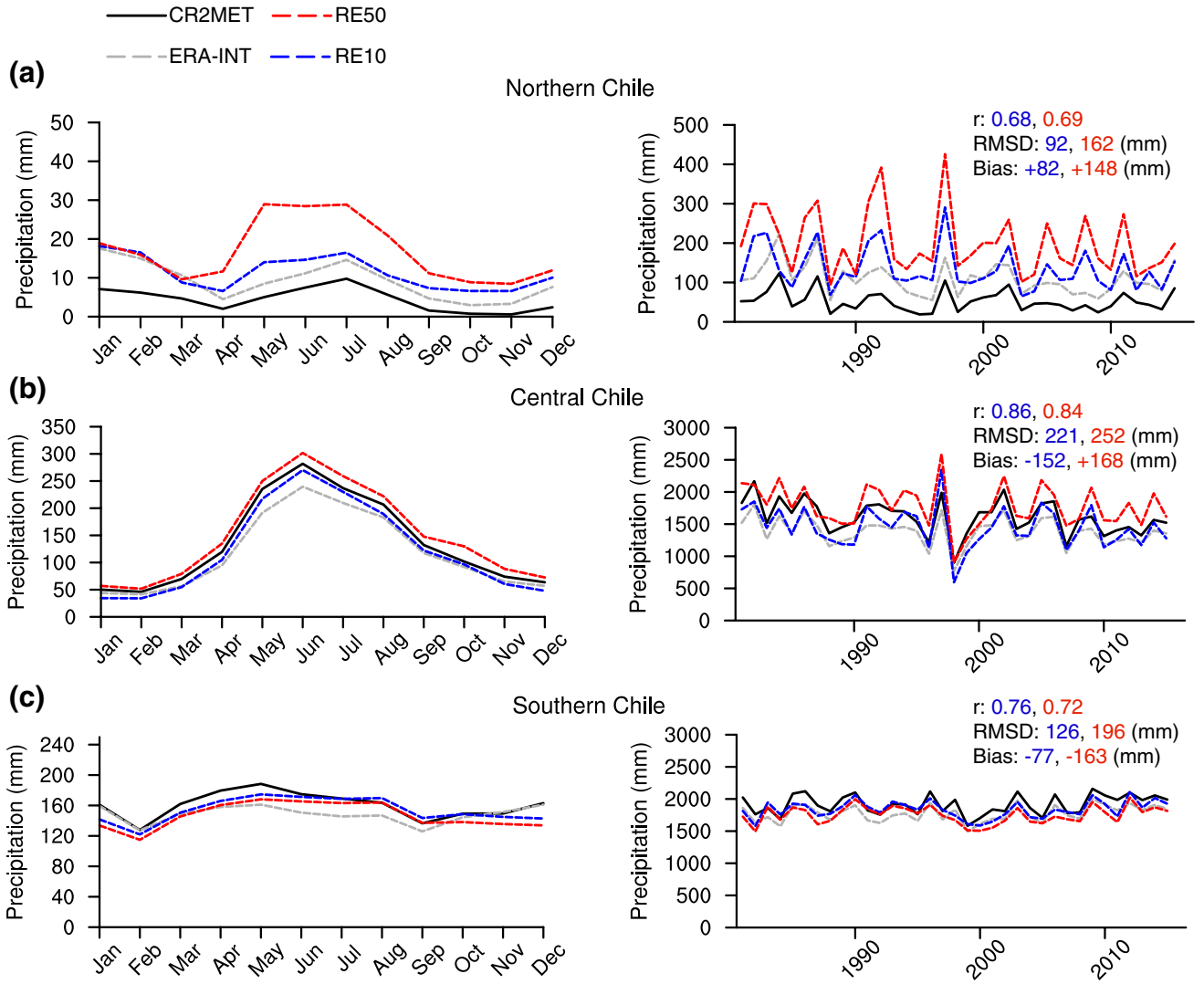

Fig. 8 **a** 36-year (1980–2015) mean annual cycle and inter-annual variability of precipitation (mm) for Northern Chile, **b** Central Chile, **c** Southern Chile. The solid line corresponds to CR2MET (black), and the dashed lines correspond to ERA-Interim (gray), dynamically downscaled simulations of ERA-Interim at 50-km (RE50, red) and 10-km (RE10, blue) resolutions

3.2 Added value analysis

3.2.1 Temperature

In this subsection, we first compare the spatial pattern of annual mean temperature (1980–2005) from MPI-ESM-MR and dynamically downscaled simulations forced with MPI-ESM-MR to those in the gridded observations (Fig. 12). Overall, compared to CR2MET, MPI-ESM-MR shows to some degree the north to south temperature gradient, however, due to the coarse resolution, it misses the east-west gradient imposed by the topography (Fig. 12b). Furthermore, it tends to underestimate temperature over the central parts of northern and central Chile. Compared to the MPI-ESM-MR and RM50, RM10 represents a closer estimation of observed temperature distribution by capturing local scale features such as warm temperatures over the Atacama Desert and east-west gradient (Fig. 12d).

A more quantitative analysis of added value for the both common grids of 0.44° and 1° indicate that there is a clear evidence of added value for temperature over the northern and central Chile (Fig. 13a). However, simulated temperature by RM10 adds more value by contrasting the features between central zone and the Andes ranges in northern and central Chile. Indeed, the ratio of amount of added value points to total points inside of each sub-region indicates larger values for RM10 in northern and central Chile. Furthermore, RM50 tends to not have added value in simulating temperature distribution over the large parts of the Central Valley and the Cordillera of central-northern Chile. When

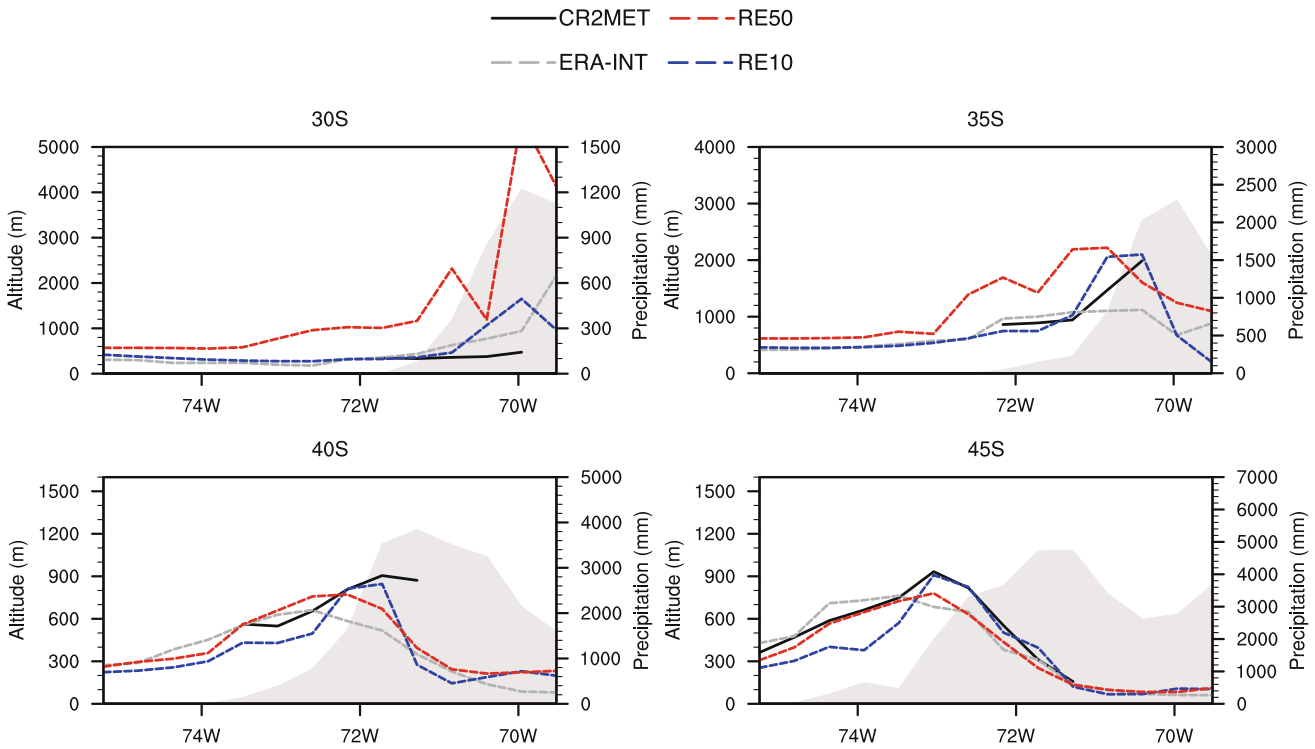

Fig. 9 36-year (1980–2015) mean annual zonal precipitation (mm) along 30°S, 35°S, 40°S and 45°S. The solid line corresponds to CR2MET (black), and the dashed lines correspond to ERA-Interim (gray), dynamically downscaled simulations of ERA-Interim at 50-km (RE50, red) and 10-km (RE10, blue) resolutions

using the 1° resolution, upscaled RM10 results again indicate that there is more evidence of added value for temperature over the northern and central Chile compared to the RM50 (Fig. 13b). Compared to the northern and central parts, both simulations show less added value over the southern Chile. It should also be noted that upscaled RM10 at a coarser resolution close to the MPI-ESM-MR resolution (1.5°) still exhibits added value in northern and central-southern Chile (Fig. S12a).

3.2.2 Precipitation

Compared to the MPI-ESM-MR and RM50, RM10 gives a closer estimation of observed precipitation distribution with a better representation of orographic precipitation, although a wet bias exists over the Andes ranges, particularly in central Chile and northern Chile (Fig. 14). A high standard deviation of annual accumulated precipitation (~ 1000 mm) within the Andes range of central Chile and Patagonian Ice Fields is also notable in RM10 (Fig. S13a). Both dynamically downscaled simulations, particularly RM10, tend to improve the MPI-ESM-MR fields in representing the spatial pattern of coefficient of variation in northern Chile except for the high Andes (Fig. S13b).

RM10 illustrates more added value and thus, it has a larger ratio of amount of added value points to total points in northern and central Chile with a marked improvement of precipitation distribution along the coastal range (Fig. 15a). However, both simulations miss added value over the Andes ranges in northern Chile indicating the difficulties improving the driving MPI-ESM-MR over these regions. Although RM50 shows significant added value over the central-southern Andes range and most parts of northern Patagonia, it has no added value over large parts of central Chile mostly along the coast and Central Valley zone. On the other hand, RM10 indicates added value due to the increased resolution along the coastal range as well as over the Andes range in central-southern Chile, highlighting the impact of the enhanced local information on the quality of the simulations. Similar spatial extent of added value exists when upscaling to the coarser common grids of 1° and 1.5°, with less added value along the coastal range of central Chile in RM10 (Figs. 15b, S12b).

We close this section with a comparison of spatial-mean daily precipitation intensity distributions from the observation, simulations and the driving MPI-ESM-MR over northern and central Chile (Fig. 16). Northern Chile is characterized by frequent low precipitation events (between 1 and 5 mm day^{-1}), and MPI-ESM-MR substantially overestimates the number of low precipitation events in northern

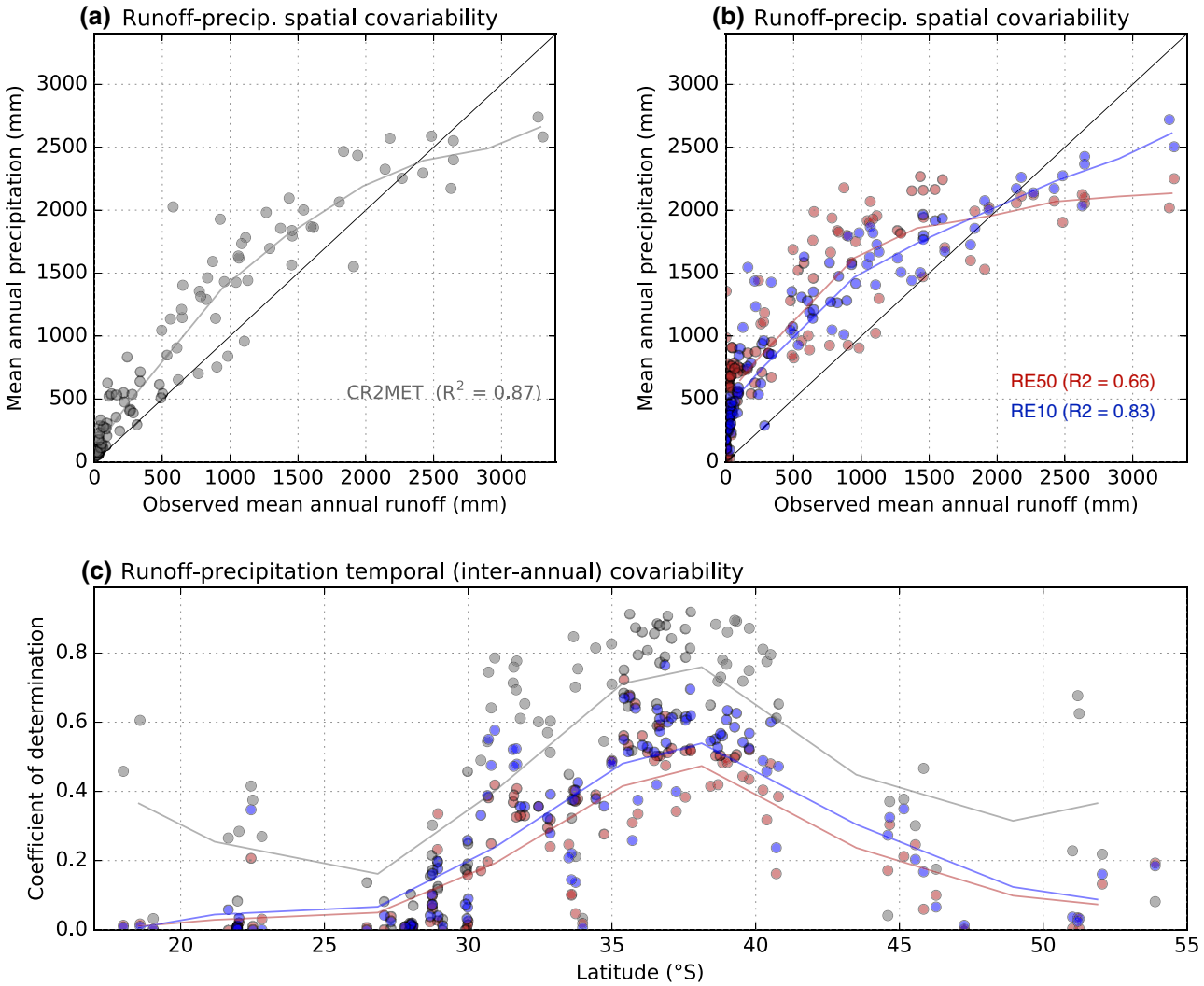

Fig. 10 **a** 36-year (1980–2015) mean annual precipitation (mm) from CR2MET against observed mean annual runoff (mm) over central Chile. **b** The same in **a** but for precipitation from dynamically downscaled simulations of ERA-Interim at 50-km (RE50, red) and 10-km (RE10, blue) resolutions. **c** Zonal distribution of coefficient of determination calculated from interannual (1980–2015) CR2MET (gray), RE50 (red) and RE10 (blue) precipitation fields against observed runoff

Chile (Fig. 16a). Both simulations, especially RM50, tend to overestimate low precipitation events, however, RM10 improves slightly the representation of number low precipitation events. In terms of extreme daily precipitation events, RM50 illustrates more frequent heavier precipitation events (> 15 mm day^{-1}), and in general, RM10 has a slightly better representation of extreme precipitation events in northern Chile. In central Chile, although low and moderate precipitation events are more frequent (between 5 and 20 mm day^{-1}) heavy precipitation events (> 45 mm day^{-1}) can be also observed (Fig. 16b). Overall, a systematic underestimation of all types of precipitation events exists in MPI-ESM-MR. The results with RM10, on the other hand, are systematically better than those of MPI-ESM-MR and give a close estimation of observed number of low and moderate precipitation events albeit with a slight overestimation. The results for extreme precipitation events indicate that both simulations represents more frequent heavier precipitation events in central Chile than what is found in reality.

4 Summary and concluding remarks

This study evaluates several simulations performed with RegCM4 over Chile. The performance of RegCM4 is evaluated through two nested hindcast simulations forced by ERA-Interim for the period 1980–2015. Added value analysis is also performed using two nested simulations forced by a global climate model (GCM, MPI-ESM-MR) for the period 1980–2005. The performance evaluations are carried

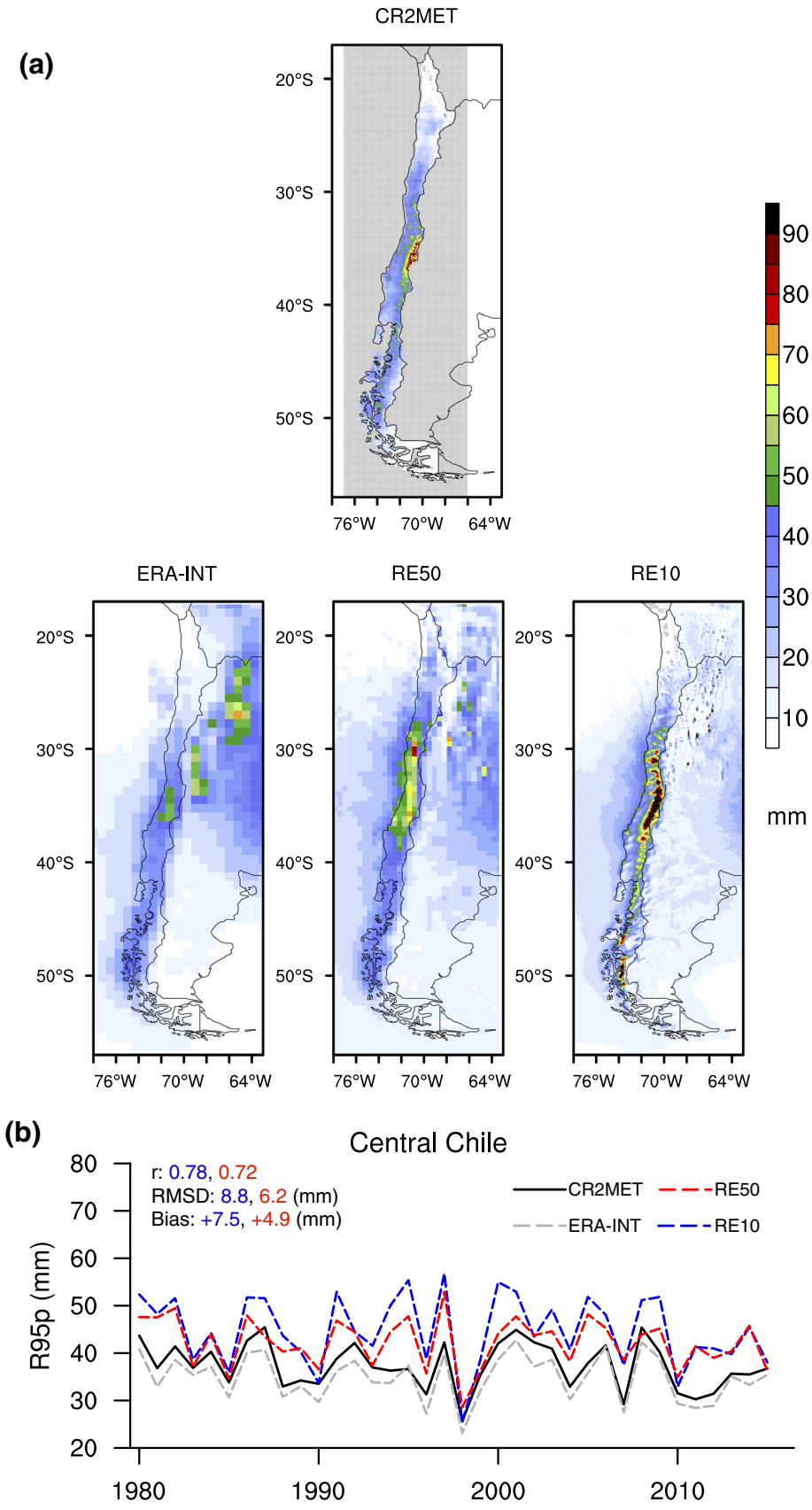

Fig. 11 **a** Spatial distribution of 36-year (1980–2015) mean annual R95 (95th percentile of the daily precipitation, mm) from CR2MET, ERA-Interim, dynamically downscaled simulations of ERA-Interim at 50-km (RE50) and 10-km (RE10) resolutions. **b** Inter-annual variability of R95 for Central Chile. The solid line corresponds to CR2MET (black), and the dashed lines correspond to ERA-Interim (gray), RE50 (red) and RE10 (blue)

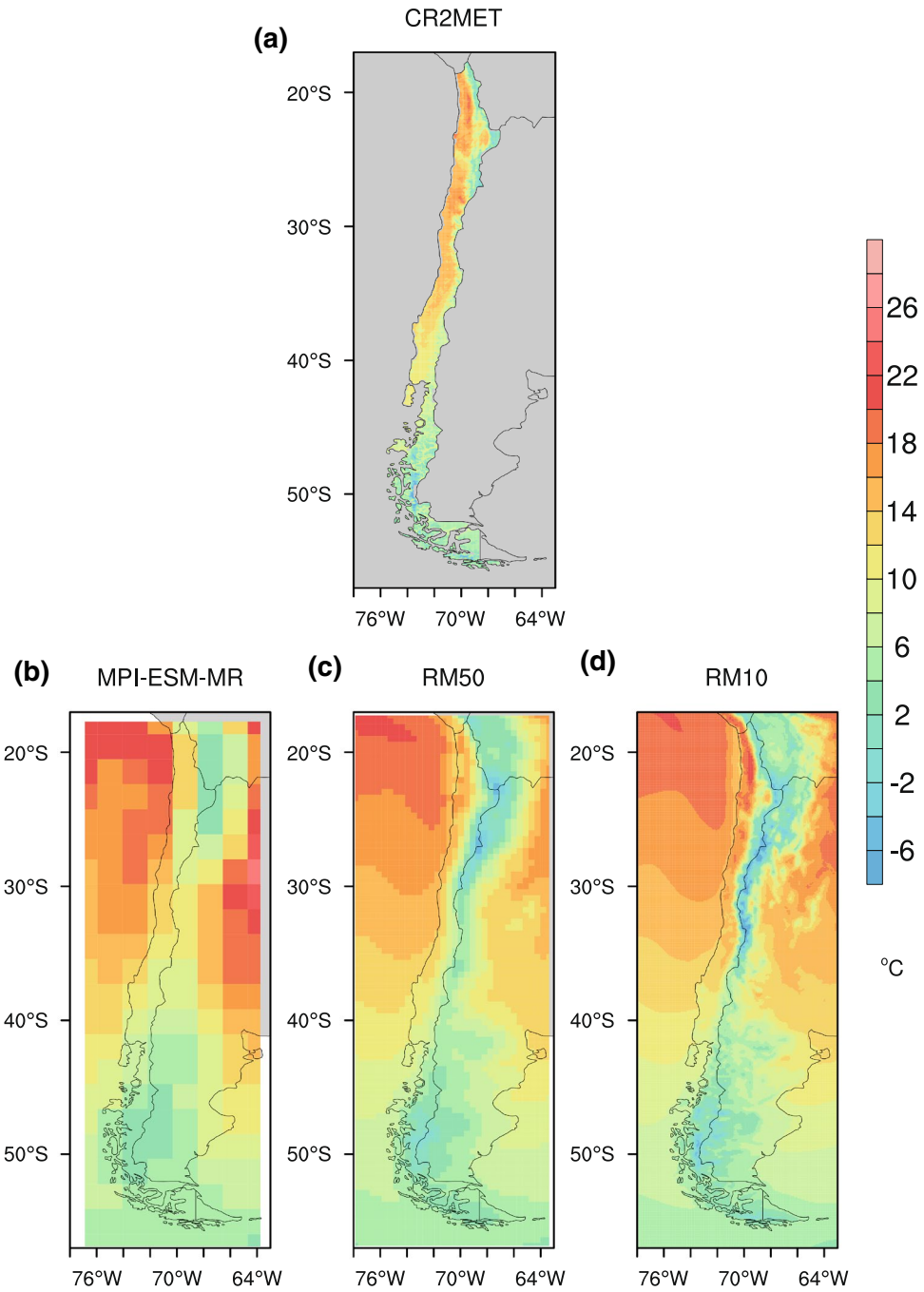

Fig. 12 **a** Spatial distribution of 26-year (1980–2005) mean annual average temperature (°C) from gridded observation (CR2MET), **b** MPI-ESM-MR, **c** dynamically downscaled simulations of MPI-ESM-MR at 50-km (RM50) and **d** 10-km (RM10) resolutions

out through a comparison of mean large-scale fields over the Pacific coast and Andes Cordillera as well as surface variables of temperature and precipitation at annual, monthly and daily time scales over three subregions of mainland Chile: Northern Chile, Central Chile, and Southern Chile. Using nested domains at 0.44° (~ 50 km, covering all South America) and 0.09° (~ 10 km, focusing on Chile) allows to analyze the role of resolution in capturing the present climate conditions (for RE50 and RE10) as well as in determining the degree of the added value (for RM50 and RM10). The simulation results were primarily compared to a high-resolution gridded meteorological observations of Chile (CR2MET) as well as to ERA-Interim. Based on the analyses, the following main findings can be highlighted:

- In general, RegCM4 shows good skills in simulating the spatial variability of mean annual temperature. However, there are some differences between the simulated and observed temperatures at local scales such as a systematic warm bias (~ + 4 °C) over the Atacama Desert in RE10.

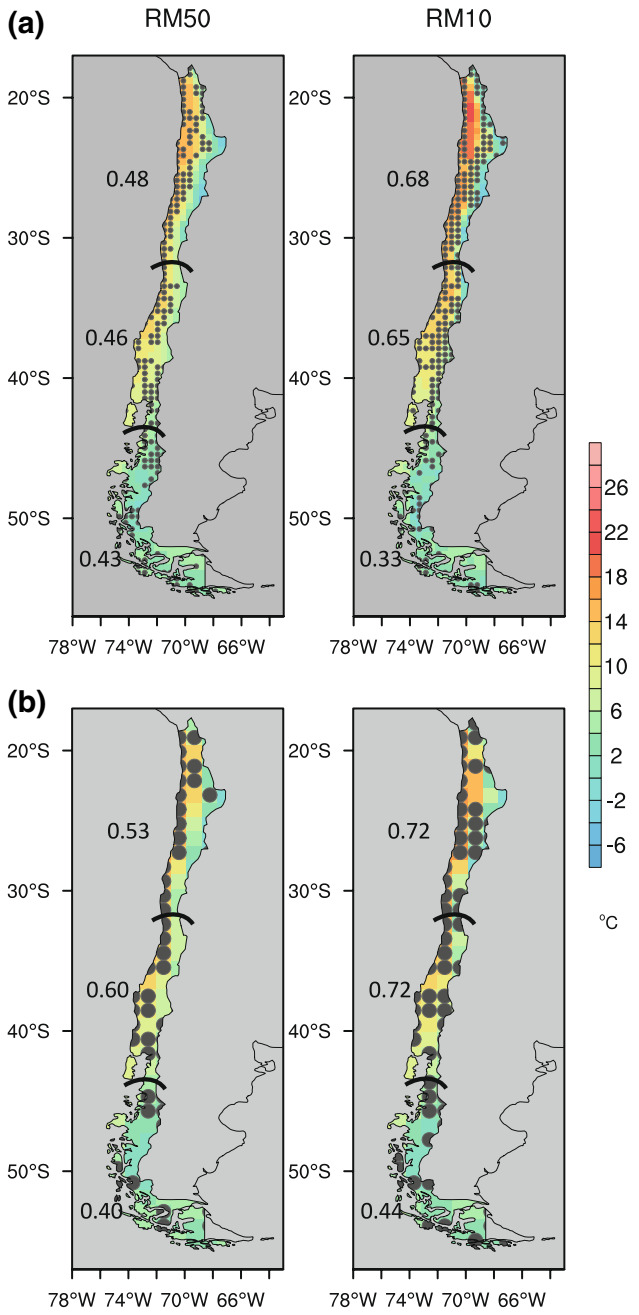

Fig. 13 **a** 26-year (1980–2005) mean annual temperature (°C) from dynamically downscaled simulations of MPI-ESM-MR at 50-km (RM50) and 10-km (RM10) resolutions. Stippling indicates grid points where there is added value by the dynamical downscaling. All datasets were remapped onto a common grid of 0.44° resolution and an elevation correction was carried out assuming a uniform temperature lapse rate of 0.65 °C/100 m, using the CR2MET topography as reference. **b** The same as **a** but with a common grid of 1° resolution. Numbers correspond to the ratio of amount of added value points to total points inside of each sub-region

- There are large discrepancies between the simulated and observed temperatures in northern Chile. Although both simulations represent the observed coastal cooling along the northern and central Chilean coasts, they largely miss the interannual variability, and RE50 does not reproduce the observed warming trend over the Andes ranges of central Chile.
- Difficulties in capturing the temperature variability in northern Chile result in even poorer representation of daily temperature extremes (i.e., 90th percentile of maximum temperature) in both simulations over this region. On the other hand, RE10 represents a better spatial and temporal variability of daily temperature extremes (i.e., frost days) over the southern Chile where the Patagonian Ice Fields are located.
- Regarding precipitation, RE10 better represents the climatology and annual cycle compared to the RE50. Furthermore, RE10 reasonably represents orographic uplift and precipitation generation on the windward side of the Andes, however, it shows a high amplitude of precipitation variability over the Andes ranges.
- Both simulations capture the spatial-mean interannual variability of precipitation in each subregion (e.g., ENSO years and mega-drought in central Chile). RE10 has a better representation of the zonal precipitation variability and for instance, it suppresses the overestimation of precipitation over the Andes Cordillera of northern Chile found in RE50.
- Compared to the ERA-Interim and RE50, RE10 represents reasonably well the spatial distribution daily precipitation extremes, although with notably larger than the observed values over the Andes in central Chile. Both simulations capture the overall spatial variability of consecutive dry days, however, with a wet bias over the Andes.
- In general, both simulations add value to those of the driving MPI-ESM-MR over large parts of Chile. However, this depends on the subregion and variable, and both simulation can exhibit different results.
- There is a clear evidence that RM10 adds more value for both temperature and precipitation in northern and central Chile. Both simulations have difficulties in improving the driving MPI-ESM-MR over the Andes ranges in northern Chile. Compared to the northern and central parts, both simulations show less added value in southern Chile.
- Frequency distribution of daily precipitation over northern and central Chile shows that RM10 adds value to the representation of extreme precipitation. For instance, it has a better performance in presenting the very dry regime of the northern Chile than that in MPI-ESM-MR and RM50 by improving the number of low precipitation events.

Our work has potentially important implications for the dynamical downscaling efforts over complex terrains

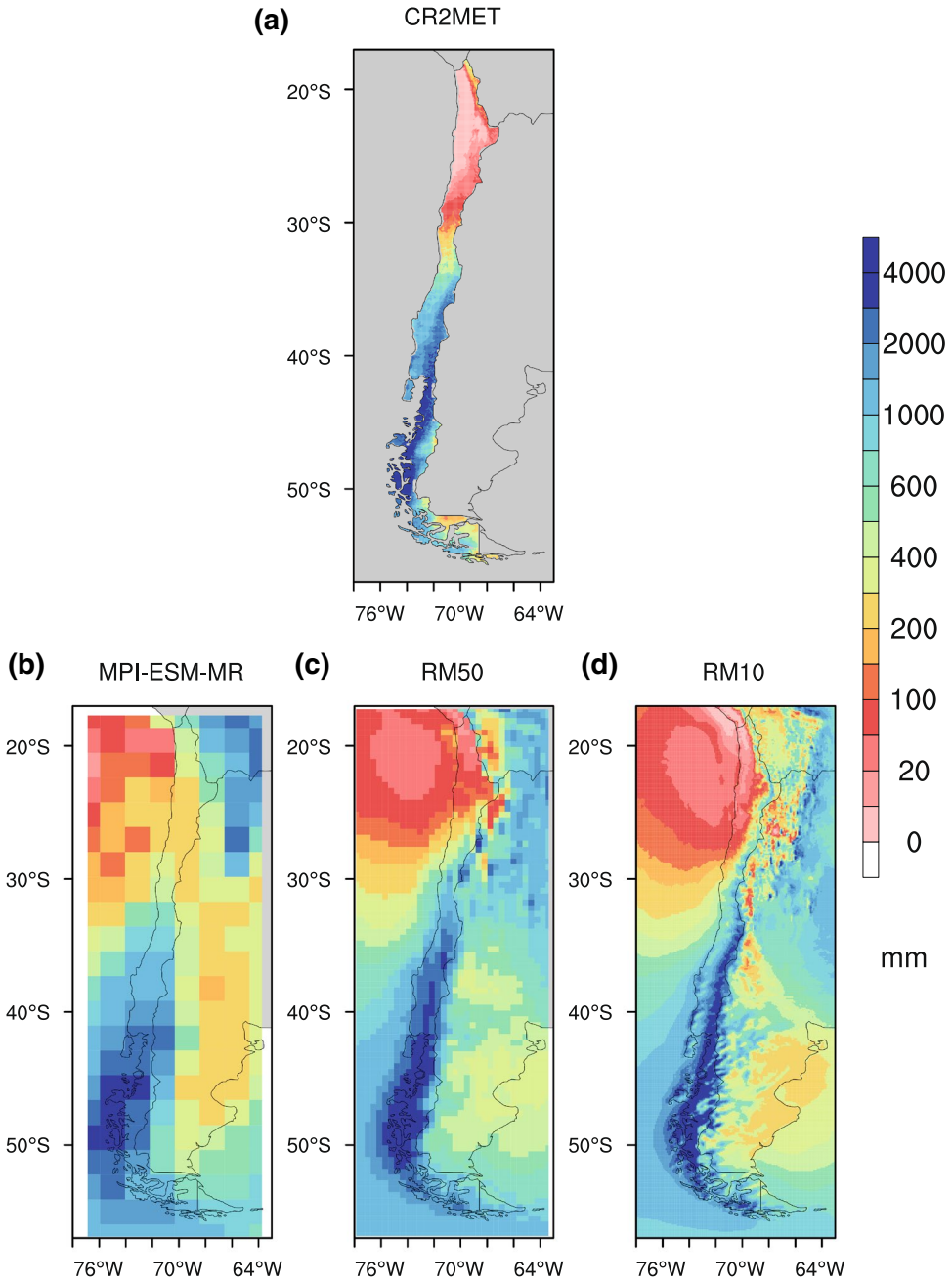

Fig. 14 **a** Spatial distribution of 26-year (1980–2005) mean annual total precipitation (mm) from gridded observation (CR2MET), **b** MPI-ESM-MR, **c** dynamically downscaled simulations of MPI-ESM-MR at 50-km (RM50) and **d** 10-km (RM10) resolutions

featuring diverse climatic gradients such as Chile. Based on the results of the present study, it could be said that coarse resolution GCMs miss important climate gradients imposed by the topography, and more importantly, this feature is shared with reanalysis products as well as medium-resolution RCM simulations (~ 50 km). Overall, high-resolution RCM simulation results (~ 10 km) are promising, and improve the representation of temperature and precipitation over Chile's complex terrain particularly in central-southern Chile. Our results also illustrate a clear evidence of the added value with the use of high-resolution RCMs suggesting that spatial resolution is critical for a better estimation of spatial and temporal variability of present climate conditions. This is in agreement with previous studies over

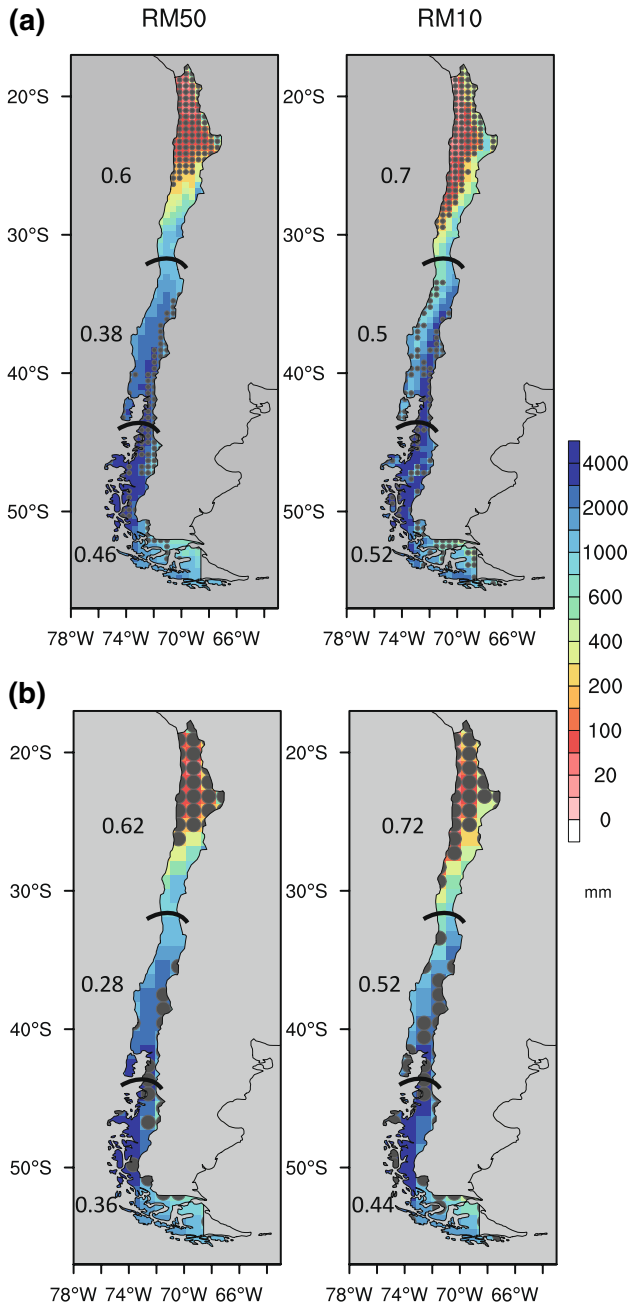

Fig. 15 **a** 26-year (1980–2005) mean annual total precipitation (mm) from dynamically downscaled simulations of MPI-ESM-MR at 50-km (RM50) and 10-km (RM10) resolutions. Stippling indicates grid points where there is added value by the dynamical downscaling. All datasets were remapped onto a common grid of 0.44° resolution. **b** The same as **a** but with a common grid of 1° resolution. Numbers correspond to the ratio of amount of added value points to total points inside of each sub-region

complex terrains in other regions (e.g., Walker and Diffenbaugh 2009; Di Luca et al. 2013; Onol 2012; Montesarchio et al. 2014; Torma et al. 2015; Shi et al. 2018).

On the other hand, some large discrepancies between the observed and simulated climate variabilities such as temperature trend contrast between coastal zone and Andes ranges of central-northern Chile, and extreme precipitation inconsistencies along the Andes Cordillera in ERA-Interim driven simulations need further investigation. These discrepancies might be due not only to model shortcomings and/or physical configuration, but also to the inadequate observational network over the regions with complex terrain. For instance, lack of sufficient and high-quality observational data over the extreme environments such as the high Andes Cordillera and Patagonia can lead to a number of potential uncertainties, and have a large impact on the robustness of the observational gridded product used as "observed truth". Similar difficulties have been highlighted in previous studies on regions with complex terrain (e.g., Onol 2012; Bozkurt et al. 2012; Solman 2013; Bieniek et al. 2016). Improving the quality of observational networks over the complex terrain can also be beneficial in implementing bias correction techniques in case of existence of persistent systematic errors in the simulated fields. Regarding modeling technique, our study suggests that beside the general improvement of climate variability via increased resolution, further efforts are required in improving the dynamical downscaling results. For instance, especially over the Andes Cordillera and Atacama Desert, model tuning and optimization are important to improve the capability of the RCM results in representing climate variability over these regions. A comparison of regional ocean-atmosphere coupled model to stand-alone RCM simulations might be needed to better resolve the impact of coastal features such as marine stratiform clouds and coastal SST forcing on the uncertainties in the simulated climate variability in northern Chile.

In conclusion, given that the highest spatial resolution of the current CORDEX-like initiatives over the South America is about 50 km and upcoming CMIP6 GCM simulations will cross the threshold of 50 km resolution, more RCM applications with higher resolutions are important to improve our understanding of the dynamical downscaling efforts over complex terrains and extreme environments. Furthermore, as the quality of the boundary conditions as well as physical configuration of RCMs play a key role in determining the robustness of the simulated fields, multi-model high-resolution RCMs forced with different GCMs are also needed, despite entailing a high computational cost. Development and continuation of CORDEX-like initiatives over the South America domain with a higher spatial resolution than the current available simulations are important to perform further model evaluation and added value analyses that may be more relevant and beneficial for the generation of more robust high-resolution climate change projections at local- and regional-scales.

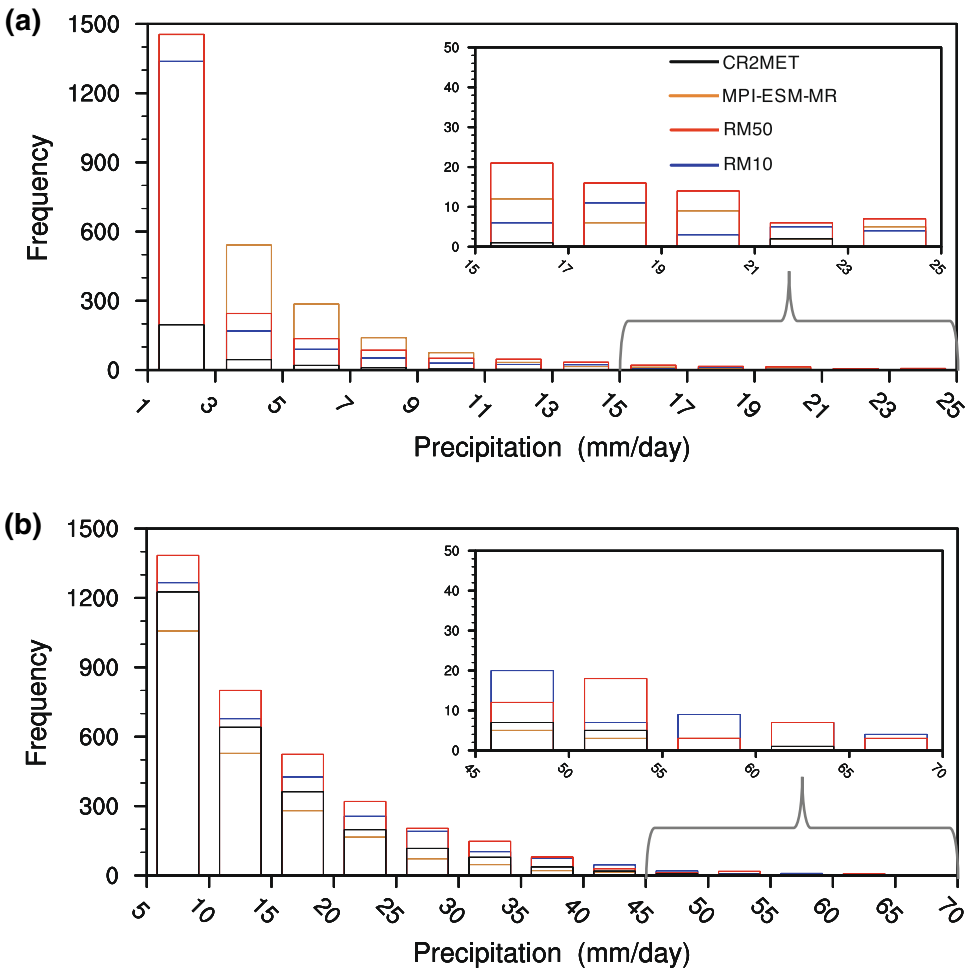

Fig. 16 **a** Histogram of frequency distribution of daily precipitation (mm, 1980–2005) for Northern Chile from CR2MET (black), MPI-ESM-MR (orange), dynamically downscaled simulations of MPI-ESM-MR at 50-km (RM50, red) and 10-km (RM10, blue) resolutions. **b** The same in **a** but for Central Chile. The calculation is based on all grid point values of the original grids of each dataset

Acknowledgements This work was funded by FONDAP-CONICYT 15110009. The authors acknowledge the anonymous reviewer for the constructive comments on the manuscript. The simulations were performed within a project entitled "Simulaciones climáticas regionales y marco de evaluación de la vulnerabilidad" funded by Chilean Ministry of Environment. A platform has been developed within that project and all the simulation outputs described in this study can be accessible from that platform following the CORDEX data format protocols, available at http://simulaciones.cr2.cl/. The authors appreciate the support from Francisca Muñoz and Nancy Valdebenito at the Data and Computing unit at (CR)2. Powered@NLHPC: This research was supported by the supercomputing infrastructure of the NLHPC (ECM-02)

References

Alvarez-Garreton C, Menzoda PA, Boisier JPea (2018) The CAMELS-CL dataset: catchment attributes and meteorology for large sample studies-Chile dataset. Hydrol Earth Syst Sci 22:5817–5846

Bieniek PA, Bhatt US, Walsh JE, Rupp TS, Zhang J, Krieger JR, Vader R (2016) Dynamical downscaling of ERA-Interim temperature and precipitation for Alaska. J Appl Meteor Climatol 55:635–654. https://doi.org/10.1175/JAMC-D-15-0153.1

Boisier JP, Rondanelli R, Garreaud R, Muñoz F (2016) Anthropogenic and natural contributions to the Southeast Pacific precipitation decline and recent megadrought in Central Chile. Geophys Res Lett 43(1):413–421. https://doi.org/10.1002/2015GL067265

Boisier JP, Alvarez-Garreton C, Cordero R, Damiani A, Gallardo L, Garreaud R, Lambert F, Ramallo C, Rojas M, Rondanelli R (2018) Anthropogenic drying in Central-Southern Chile evidenced by long-term observations and climate model simulations. Elem Sci Anth. https://doi.org/10.1525/elementa.328

Bozkurt D, Turuncoglu U, Sen OL, Dalfes HN (2012) Downscaled simulations of the ECHAM5, CCSM3 and HadCM3 global models for the Eastern Mediterranean-Black Sea region: evaluation of the reference period. Clim Dyn 39(1–2):207–225. https://doi.org/10.1007/s00382-011-1187-x

Bozkurt D, Rondanelli R, Garreaud R, Arriagada A (2016) Impact of warmer eastern tropical Pacific SST on the March 2015 Atacama floods. Mon Weather Rev 144(11):4441–4460

Bozkurt D, Rojas M, Boisier JP, Valdivieso J (2018a) Projected hydroclimate changes over Andean basins in central Chile from downscaled CMIP5 models under the low and high emission scenarios. Clim Change 150(3–4):131–147. https://doi.org/10.1007/s10584-018-2246-7

Bozkurt D, Rondanelli R, Marín J, Garreaud R (2018b) Foehn event triggered by an atmospheric river underlies record-setting temperature along continental Antarctica. J Geophys Res Atmos 128(3):3871–3892. https://doi.org/10.1002/2017JD027796

Carril A, Menéndez C, Remedio A et al (2012) Assessment of a multi-RCM ensemble for South Eastern South America. Clim Dyn 39:2747–2768

Comin AN, Schumacher V, Justino F, Fernrández A (2018) Impact of different microphysical parameterizations on extreme snowfall events in the Southern Andes. Weather Clim Extrem. https://doi.org/10.1016/j.wace.2018.07.001

Coppola E, Giorgi F, Raffaele F, Fuentes-Franco R, Giuliani G, LLopart-Pereira M, Mamgain A, Mariotti L, Diro GT, Torma C (2014) Present and future climatologies in the phase i CREMA experiment. Clim Change 125(1):23–38. https://doi.org/10.1016/j.atmosenv.2011.02.001

Dee DP, Uppala SM, Berrisford P, Poli P, Kobayashi S, Andrae U, Balmaseda MA, Balsamo G, Bauer P, Bechtold P, Beljaars ACM, van de Berg L, Bidlot J, Bormann N, Delsol C, Dragani R, Fuentes M, Geer AJ, Haimberger L, Healy SB, Hersbach H, Hólm EV, Isaksen L, Káallberg P, Káhler M, Matricardi M, McNally AP, Monge-Sanz BM, Morcrette JJ, Park BK, Peubey C, de Rosnay P, Tavolato C, Thépaut JN, Vitart F (2011) The ERA-Interim reanalysis: configuration and performance of the data assimilation system. Q J R Meteorol Soc 137:553–597

Demaria EMC, Maurer EP, Thrasner B, Vicuñna S, Meza F (2013) Climate change impacts on an Alpine Watershed in Chile: do new model projections change the story? J Hydrol 502:128–138. https://doi.org/10.1016/j.jhydrol.2013.08.027

DGA (2017) Actualización del balance hídrico nacional. Tech. Rep. SIT No. 417, Ministerio de Obras Públicas, Dirección General de Aguas, División de Estudios y Planificación, Santiago, Chile. Realizado por Universidad de Chile and Pontificia Universidad Católica de Chile

Di Luca A, Elia R, Laprise R (2013) Potential for small scale added value of RCMs downscaled climate change signal. Clim Dyn 40(3–4):601–618. https://doi.org/10.1007/s00382-012-1415-z

Di Luca A, Argueso D, Evans JP, Laprise R (2016) Quantifying the overall added value of dynamical downscaling and the contribution from different spatial scales. J Geophys Res Atmos 121(4):1575–1590. https://doi.org/10.1002/2015JD024009

Dickinson RE, Henderson-Sellers A, Kennedy PJ (1993) Biosphere-atmosphere transfer scheme (BATS) Version 1e as coupled to the NCAR Community Climate Model. NCAR Tech. Note NCAR/TN-387+STR, NCAR, Boulder

Falco M, Carril AF, Menéndez CG, Zaninelli PG, Li LZX (2018) Assessment of CORDEX simulations over South America: added value on seasonal climatology and resolution considerations. Clim Dyn. https://doi.org/10.1007/s0038

Falvey M, Garreaud R (2009) Regional cooling in a warming world: recent temperature trends in the Southeast Pacific and along the west coast of subtropical South America (1979–2006). J Geophys Res Atmos 114(D04):102

Fritsch JM, Chappell CF (1980) Numerical prediction of convectively driven mesoscale pressure systems. I. Convective parameterization. J Geophys Res 37:1722–1733

Gallardo L, Olivares G, Langner J, Aarhus B (2002) Coastal lows and sulfur air pollution in Central Chile. Atmos Environ 36(23):3829–3841

Garreaud R (2009) The Andes climate and weather. Adv Geosci 7:1–9

Garreaud R, Lopez P, Minvielle M, Rojas M (2010) Large-scale control on the Patagonian climate. Earth Planet Sci Lett 292:39–50. https://doi.org/10.1016/j.epsl.2010.01.017

Garreaud R, Molina A, Farias M (2013) Andean uplift, ocean cooling and Atacama hyperaridity: a climate modeling perspective. J Clim 26(1):215–230. https://doi.org/10.1175/JCLI-D-12-00001.1

Garreaud R, Falvey M, Montecinos A (2016) Orographic precipitation in coastal southern Chile: mean distribution, temporal variability, and linear contribution. J Hydrometeor 17:1185–1202

Garreaud R, Alvarez-Garreton C, Barichivich J, Boisier JP, Duncan C, Galleguillos M, Zambrano-Bigiarini M (2017) The 2010–2015 mega drought in Central Chile: impacts on regional hydroclimate and vegetation. Hydrol Earth Syst Sci 21:6307–6327

Giorgetta MA et al (2013) Climate and carbon cycle changes from 1850 to 2100 in MPI-ESM simulations for the Coupled Model Intercomparison Project phase 5. J Adv Model Earth Syst 5(3):572–597

Giorgi F, Marinucci MR, Bates GT (1993a) Development of a second generation regional climate model (RegCM2). Part I: Boundary layer and radiative transfer processes. Mon Weather Rev 121:2794–2813. https://doi.org/10.1175/1520-0493(1993)121<2794:DOASGR>2.0.CO;2

Giorgi F, Marinucci MR, Bates GT, DeCanio G (1993b) Development of a second generation regional climate model (RegCM2). Part II: Convective processes and assimilation of lateral boundary conditions. Mon Weather Rev 121:2814–2832. https://doi.org/10.1175/1520-0493(1993)121<2814:DOASGR>2.0.CO;2

Giorgi F, Jones C, Asrar GR (2009) Addressing climate information needs at the regional level: the CORDEX framework. WMO Bull 58:175–183

Giorgi F, Coppola E, Solmon F, Mariotti L, Sylla MB, Bi X, Elguindi N, Diro GT, Nair V, Giuliani G, Turuncoglu UU, Cozzini S, Guttler I, O'Brien TA, Tawfik AB, Shalaby A, Zakey AS, Steiner AL, Stordal F, Sloan LC, Brankovic C (2012) RegCM4: model description and preliminary tests over multiple CORDEX domains. Clim Res 52:7–29. https://doi.org/10.3354/cr01018

Giorgi F, Torma C, Coppola E, Ban N, Schar C, Somot S (2016) Enhanced summer convective rainfall at Alpine high elevations in response to climate warming. Nat Geosci 9:584–589. https://doi.org/10.1038/ngeo2761

Grassi B, Redaelli G, Visconti G (2013) Arctic sea ice reduction and extreme climate events over the Mediterranean region. J Clim 26:10,101–10,110

Grell GA (1993) Prognostic evaluation of assumptions used by Cumulus parameterizations. Mon Weather Rev 121:764–787

Grell GA, Dudhia J, Stauffer DR (1994) Description of the fifth generation Penn State/NCAR Mesoscale Model (MM5). NCAR Tech. Note NCAR/TN-398+STR, NCAR, Boulder

Guttler I, Stepanov I, Branković C, Nikulin G, Jones C (2015) Impact of horizontal resolution on precipitation in complex orography simulated by the Regional Climate Model RCA3. Mon Weather Rev 143:3610–3627. https://doi.org/10.1175/MWR-D-14-00302.1

Holtslag AAM, de Bruijn EIF, Pan HL (1990) A high resolution air mass transformation model for short-range weather forecasting. Mon Weather Rev 118:1561–1575. https://doi.org/10.1175/1520-0493(1990)118<1561:AHRAMT>2.0.CO;2

Jones C, Giorgi F, Asrar GR (2011) The coordinated regional downscaling experiment: CORDEX, an international downscaling link to CMIP5. CLIVAR Exch 16:34–40

Jones PW (1999) First- and second-order conservative remapping schemes for grids in spherical coordinates. Mon Weather Rev 127:2204–2210

Karl TR, Nicholls N, Ghazi A (1999) CLIVAR/GCOS/WMO workshop on indices and indicators for climate extremes: workshop summary. Clim Change 42:3–7

Kato S, Loeb NG, Rose FG, Doelling DR, Rutan DA, Caldwell TE, Yu L, Weller RA (2013) Surface irradiances consistent with ceres-derived top-of-atmosphere shortwave and longwave irradiances. J Clim 26:2719–2740. https://doi.org/10.1175/JCLI-D-12-00436.1

Kiehl JT, Hack JJ, Bonan GB, Boville BA, Breigleb BP, Williamson D, Rasch P (1996) Description of the NCAR Community Climate Model (CCM3). NCAR Tech. Note NCAR/TN-420+STR, NCAR, Boulder

Lenaerts JTM, van den Broeke MR, van Wessem JM, van de Berg WJ, van Meijgaard E, van Ulft LH, Schaefer M (2014) Extreme precipitation and climate gradients in patagonia revealed by high-resolution regional atmospheric climate modeling. J Clim 27:4607–4621. https://doi.org/10.1175/JCLI-D-13-00579.1

Marcella MP, Eltahir EA (2012) Modeling the summertime climate of Southwest Asia: the role of land surface processes in shaping the climate of semiarid regions. J Clim 25(2):704–719. https://doi.org/10.1175/2011JCLI4080.1

Martens B, Miralles DG, Lievens H, van der Schalie R, de Jeu RAM, Fernandez-Prieto D, Beck HE, Dorigo WA, Verhoest NEC (2017) Gleam v3: satellite-based land evaporation and root-zone soil moisture. Geosci Model Dev 10:1903–1925. https://doi.org/10.5194/gmd-2016-162

Mazzeo A, Huneeus N, Ordoñez C, Orfanoz-Cheuquelaf A, Menut L, Mailler S, Valari M, van der Gon HD, Gallardo L, Muñoz R, Donoso R, Galleguillos M, Osses M, Tolvett S (2018) Impact of residential combustion and transport emissions on air pollution in santiago during winter. Atmos Environ 190:195–208. https://doi.org/10.1016/j.atmosenv.2018.06.043

Middleton N (2003) Going to extremes. Pan Books, London

Montesarchio M, Zollo AL, Bucchignani E, Mercogliano P, Castellari S (2014) Performance evaluation of high-resolution regional climate simulations in the Alpine space and analysis of extreme events. J Geophys Res Atmos 119:3222–3237. https://doi.org/10.1002/2013JD021105

Onol B (2012) Effects of coastal topography on climate: high-resolution simulation with a regional climate model. Clim Res 52:159–174. https://doi.org/10.3354/cr01077

Pal JS, Small EE, Eltahir EAB (2000) Simulation of regional-scale water and energy budgets: representation of surged cloud and precipitation processes within RegCM. J Geophys Res 105:29,579–29,594

Peterson TC, et al (2001) Report on the activities of the working group on climate change detection and related rapporteurs 1998-2001. WMO Tech. Report Rep. WCDMP-47, WMO-TD 1071, WMO, Geneve, Switzerland

Rojas M (2006) Multiply nested regional climate simulation for southern South America: sensitivity to model resolution. Mon Weather Rev 134:2208–2223. https://doi.org/10.1175/MWR3167.1

Rutllant J, Fuenzalida H (1991) Synoptic aspects of the central Chile rainfall variability associated with the Southern Oscillation. Int J Climatol 11:63–76

Rutllant J, Fuenzalida H, Aceituno P (2003) Climate dynamics along the arid northern coast of Chile: The 1997–1998 Diclima Experiment. J Geophys Res 108:4538–4542

Saide PE, Carmichael GR, Spak SN, Gallardo L, Osses AE, Mena-Carrasco MA, Pagowski M (2011) Forecasting urban PM10 and PM2.5 pollution episodes in very stable nocturnal conditions and complex terrain using WRF-Chem CO tracer model. Atmos Environ 45:2769–2780. https://doi.org/10.1016/j.atmosenv.2011.02.001

Schmitz R (2005) Modelling of air pollution dispersion in Santiago de Chile. Atmos Environ 39(11):2035–2047

Shi Y, Wang G, Gao X (2018) Role of resolution in regional climate change projections over China. Clim Dyn 51(5–6):2375–2396. https://doi.org/10.1007/s0038

Silvestri G, Vera C (2009) Nonstationary impacts of the southern annular mode on Southern Hemisphere climate. J Clim 22(22):6142–6148

Solman SA (2013) Regional climate modeling over South America: a review. Adv Meteor 2013:1–13. https://doi.org/10.1155/2013/504357

Solman SA, Sanchez E, Samuelsson P, da Rocha RP, Li L, Marengo J, Pessacg NL, Remedio ARC, Chou SC, Berbery H, Le Treut H, de Castro M, Jacob D (2013) Evaluation of an ensemble of regional climate model simulations over South America driven by the ERA-Interim reanalysis: model performance and uncertainties. Clim Dyn 41(5–6):1139–1157

Torma C, Giorgi F, Coppola E (2015) Added value of regional climate modeling over areas characterized by complex terrain: precipitation over the Alps. J Geophys Res Atmos 120(9):3957–3972. https://doi.org/10.1002/2014JD022781

Viale M, Garreaud R (2015) Orographic effects of the subtropical and extratropical Andes on upwind precipitating clouds. J Geophys Res Atmos 120:4962–4974. https://doi.org/10.1002/2014JD023014

Viale M, Houze RA, Rasmussen KL (2013) Upstream orographic enhancement of a narrow cold-frontal rainband approaching the Andes. Mon Weather Rev 141:1708–1730. https://doi.org/10.1175/MWR-D-12-00138.1

Vuille M, Franquist E, Garreaud R, Casimiro WSL, Cáceres B (2015) Impact of the global warming hiatus on Andean temperature. J Geophys Res Atmos 120(9):3745–3757

Walker MD, Diffenbaugh NS (2009) Evaluation of high-resolution simulations of daily-scale temperature and precipitation over the United States. Clim Dyn 33:1131–1147

Zeng X, Zhao M, Dickinson RE (1998) Intercomparison of bulk aerodynamic algorithms for the computation of sea surface fluxes using TOGA COARE and TAO data. J Clim 11:2628–2644. https://doi.org/10.1175/1520-0442(1998)011<2628:IOBAAF>2.0.CO;2